Accelerated Testing Method to Estimate the Lifetime of Polyethylene Pipes

Roozbeh Kalhor

Thesis submitted to the faculty of the
Virginia Polytechnic Institute and State University in partial fulfillment of the requirements
for the degree of

Master of Science
in
Macromolecular Science and Engineering

Scott W. Case, Chair
Donald G. Baird
Michael J. Bortner

February 14, 2017
Blacksburg, VA

Keywords: creep characterization, long-term hydrostatic strength (LTHS), plastic pipe, ductile failure, time-temperature superposition, digital image correlation (DIC), small angle X-ray scattering (SAXS), and wide angle X-ray diffraction (WAXD)

Accelerated Testing Method to Estimate the Lifetime of Polyethylene Pipes

Roozbeh Kalhor

ABSTRACT

The ability to quickly develop predictions of the time-to-failure under different loading levels allows designers to choose the best polymeric material for a specific application. Additionally, it helps material producers to design, manufacture, test, and modify a polymeric material more rapidly. In the case of polymeric pipes, previous studies have shown that there are two possible time-dependent failure mechanisms corresponding to ductile and brittle failure. The ductile mechanism is evident at shorter times-to-failure and results from the stretching of the amorphous region under loading and the subsequent plastic deformation. Empirical results show that many high-performance polyethylene (PE) materials do not exhibit the brittle failure mechanism. Hence, it is critical to understand the ductile mechanism and find an approach to predict the corresponding times-to-failure using accelerated means. The aim of this study is to develop an innovative rupture lifetime acceleration protocol for PE pipes which is sensitive to the structure, orientation, and morphology changes introduced by changing processing conditions. To accomplish this task, custom fixtures are developed to admit tensile and hoop burst tests on PE pipes. A pressure modified Eyring flow equation is used to predict the rupture lifetime of PE pipes using the measured mechanical properties under axial tensile and hydrostatic pressure loading in different temperatures and strain rates. In total, the experimental method takes approximately one week to be completed and allows the prediction of pipe lifetimes for service lifetime in excess of 50 years.

Accelerated Testing Method to Estimate the Lifetime of Polyethylene Pipes

Roozbeh Kalhor

GENERAL AUDIENCE ABSTRACT

Steel, cast and galvanized iron, and asbestos cement (AC) pipelines have been historically used in water management services. However, they often experienced deterioration because of corrosion and encrustation, resulting in 23 to 27 bursts per 100 miles of pipeline in the US per year. Therefore, plastic pipes were developed to carry liquids (water and sewage), gases, etc. The Plastic Pipe Institute (PPI) requires a service life of at least 50-years for plastic pipes. Hence, pipe producers and material suppliers continuously attempt to improve the materials and manufacturing processes used for plastic pipes to increase their service lifetimes. However, there is still no plastic pipe that has been in service for 50 years. Therefore, a few techniques have been developed to accelerate the aging process and to predict if the plastic pipe is able to endure the 50-year lifetime without failure.

In this work, a combined experimental and analytical framework is presented to develop accelerated lifetime estimates for plastic pipes. Custom axial tensile and internal pressurization fixtures are developed to measure the pipe response; the analytical method is used to extend the results to predict 50-year (and beyond) behavior.

To my parents: Shohreh and Asghar
Thank you for your endless support in this journey
For keeping faith on me
For being there when I needed you

Thank you for everything

Acknowledgements

I would like to express my sincere gratitude to my advisor, Dr. Scott W. Case, for his endless support during my M.S. in MACR program and my Ph.D. in EM program, for his patience, motivation, and immense knowledge. He gave me the room and opportunity to try different areas, to fail, and to find the way for which I was truly passionate. I could not have imagined having a better advisor and mentor.

I would like to express my appreciation to my committee members; Dr. Donald G. Baird and Dr. Michael Bortner for their advice, encouragement, and insightful comments.

Last but not least, my sincere thanks goes to

- BEAM staff including Mac McCord, Danny Reed, Darrel Link, and Beverly Williams.
- Dr. Robert B. Moore and Greg B. Fahs: for their involvement in the project and their assistance on characterization process.
- Cincinnati Technology Center of LyondellBasell Industries: for funding the project, providing required information and materials, and their continuous support.

Table of Contents

List of Figures

List of Tables

Chapter 1

1. Introduction

1.1. Background

Plastic pipes were recently developed to carry liquids and gases of their moderate cost, ease of handling and installation (lightweight and lower labor requirement), long service life, reduced long-term maintenance and replacement costs and resistance to degradation caused by moisture, ultraviolet radiation, and chemicals compared with materials such as corrugated steel, concrete, and ductile iron. As a result, plastic pipe industry is predicted to grow with double-digit rate over next ten years and reach $500 billion by 2024, worldwide. Yet alone, in the US, sales is expected to reach $57.3 billion and total of 11.8 billion feet of pipe [1]. The shift in US energy policy to produce natural gas, as an environmentally friendly substitute to coal, is just one of the reasons for boosting plastic pipe demand. In fact, line plastic pipes are utilized to transfer and distribute oil/gas from wellheads to power plants and residential market.

Polyethylene (PE), Polyvinyl chloride (PVC), polypropylene (PP), and polybutylene (PB) are among the polymers which are commonly used as the based material for plastic pipes. Ethylene is a simple monomer which consists of two carbon atoms with two hydrogen atoms attached to each carbon. The polymerization process to produce Polyethylene requires low temperature, low pressure, suitable catalysts, and co-monomers [2]. PE can be classified as: (1) High Density Polyethylene (HDPE), linear Polyethylene, (2) Medium Density Polyethylene (MDPE) (3) Low Density Polyethylene (LDPE), branched PE, and (4) Crosslinked Polyethylene. The shorter the chains and the lower the degree of branching, the better crystallization (spherulites formation) occurs when PE melt cools down. As a result, HDPE because of having shorter chains and lower degree of branching has greater degree of

crystallinity and higher density (Table 1-1) [3]. As a result, HDPE has the second largest share in the plastic pipe business.

Table 1-1. PE classification based on density and percentage of crystallization

	Density	Degree of crystallinity
HDPE	0.94 to 0.965 g/cm^3	60-80%
MDPE	0.93 to 0.94 g/cm^3	50-60%
LDPE	0.915 to 0.93 g/cm^3	35-50%

There are number of factors which affect the PE properties including crystallinity, molecular weight, molecular weight distribution, degree of branching in the molecular chain, and the length of side chains. Yield stress, modulus of elasticity, hardness and solvent resistance are among the properties which increase with increasing PE density (the degree of crystallinity). However, increasing density has a detrimental effect on impact strength, transparency, and stress cracking resistance. Increasing molecular weight of PE increases its impact strength, tensile strength, elongation at break, and finally stress cracking resistance.

One of the most important properties of plastic pipes is their hydrostatic strength (stress leading to rupture) or service life under internal pressure. The hoop stress as the equivalent mechanical term for hydrostatic strength, σ_H, can be related to internal pressure, P, as follows

$$\sigma_H = \frac{P\ d_n}{2\ t}$$

in which d_n is the nominal diameter and t is thickness. In general, hydrostatic strength is related to loading rate, loading period, and temperature [4]. Figure 1-1 shows a plot of creep rupture strength versus time-to-failure of actual pipes which are pressurized with water and submerged in a water bath. Three stages of plastic pipe failure was previously addressed as (1) ductile failure, as a result of plastic strain accumulation (2) brittle failure, as a result of slow crack propagation, and (3) brittle failure, as a result of thermo-oxidation degradation (aging) [4-6]. Figure 1-1 also shows that hydrostatic (burst) testing of plastic pipes at 80°C may demonstrate a possible transition (inflection) from ductile to brittle failure known as the “knee” in a shorter amount of time.

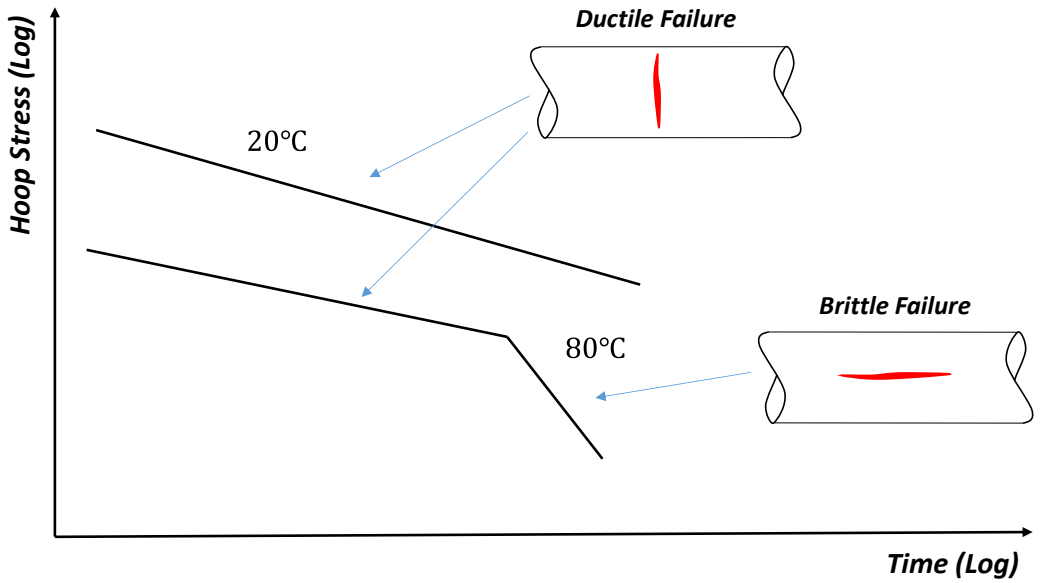

Figure 1-1. Qualitative illustration of internal creep rupture strength versus time to failure

1.2. Ductile failure

Ductile failure in PE pipes occurs when the stress level is relatively high comparable to the yield point of the polymer. It occurs in a short period of time with localized expansion of the pipe (the final shape is similar to a balloon). In fact, the failure resembles start of necking in a tensile testing in which engineering stress (load over initial area) reaches a maximum point (yield point). For polymers, the yield point is defined when the derivative of engineering strain with respect to time, $\frac{d\varepsilon}{dt}$, is equal to zero. After yielding point, necking occurs, leading to a decrease in the initial cross-sectional area. However, load over the instantaneous area (true stress) remains nearly constant during this drawing process. For polyethylene, the tensile behavior is affected by the semi-crystalline nature of the material. Before yielding, the amorphous region starts to stretch but load is carried by both crystalline and amorphous regions. After yielding, the deformation is as result of amorphous phase rearrangement and lamellae slipping past each other in the direction of loading. However, each lamella is still undamaged. At the onset of the strain hardening region, the lamellae start to break and unfold, resulting in a rough fibrous surface. The condition continues and leads to material failure [7]. In general, the plastic region is a result of chains being stretched, rotated, sled, and disentangled under load.

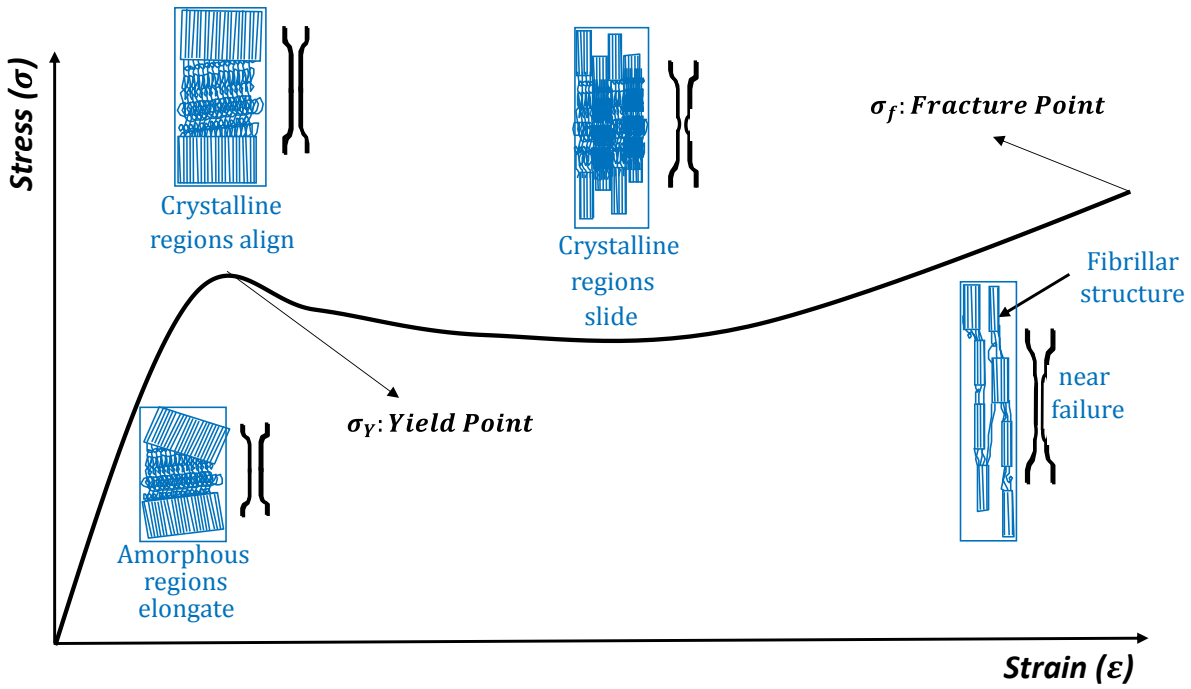

Figure 1-2. Tensile stress-strain curve of a polymer and related structural deformation at each stage [8]

Two most common standards to determine the long-term hydrostatic strength of polymeric pipes are (1) ASTM D2837 which is the dominant methodology in North America and developed by Hydrostatic Stress Board of Plastic Pipe Institute (PPI) [9] and (2) ISO 9080 [10]. The D2837 test requires a minimum of 18 pipe specimens to be tested in which one sample have to be placed under hydrostatic pressure for more than 10,000 hours to produce the expected strength for 100,000 hours.

Plastic Pipe Institute (PPI) requires a service life of at least 50-years for plastic pipes. However, plastic pipes were developed in recent decades and there is no actual data on HDPE pipes in room temperature under regular water pressure exceeding the 50-years period. To accelerate the process of ageing, some techniques have been developed which use Arrhenius equation to predict the time-to-failure of the pipes. Based on the equation, it is possible to extrapolate the creep strength of plastic pipes in lower temperature (i.e. room temperature) at longer times using the measurement at higher temperatures but in shorter amount of time. For example, EN ISO 9080 standard requires 10,000 hours (more than 13 months) to measure the minimal required strength (MRS) or long-term hydrostatic strength (LTHS) at

room temperature of a plastic pipe to pass the time-to-failure limit of 50-years. While this represents substantial acceleration in comparison to 50-years, it is still extremely time-consuming.

The EN ISO 9080 starts with creep strength measurement of plastic pipes which be evaluated by the Standard Extrapolation Method (SEM) using following equation

$$Log\,[t] = -A - \frac{B}{T} Log\,[\sigma] + \frac{C}{T} + D\ Log\,[\sigma]$$

The LTHS and the 97.5% Lower Prediction Limit (LPL) can be obtained at operating temperature over the course of 50 years [3]. The basis of the LPL value is the Renard 10 number series (R 10) for values under 10 MPa and the R 20 number series for values more than 10 MPa. By dividing a decade to 10 or 20 equal parts on log-log scale, the standard (rounded) number series (ISO 3) can be acquired as follow

$$Rounded\ number\ series: 1, 1.25, 1.6, 2, 3.2, 4, 5, 6.3, 8, 10, 11.2, 12.5, 14, 16, etc.$$

For instance, the calculated LPL value for the Hostalen CRP 100 black produced by Basell Company, 11 MPa, is rounded down to the closest rounded Renard number which is 10 MPa. The resulting number is called the Minimum Required Strength (MRS) which is the basis for naming PE pipes. Basell produces PE pipes with two MRS values as summarized in Table 1-2.

Table 1-2. MRS values for 2 different class of PE pipes

Class	MRS (MPa)
PE 100	10
PE 80	8

1.3. Brittle failure

Brittle fracture usually initiates due to a very high localized stress from small defects (stress concentration points) or in-homogeneities in the pipe wall such as impingements, voids, etc. The resulting crack propagates along the pipe length. The resistance to slow crack propagation depends on average molecular weight, molecular weight distribution, copolymer content and distribution. PE slows the crack propagation by crazing zone formation which includes highly oriented craze fibrils [3]. The Full Notch Creep Test (FNCT)

(ISO/CD 16670) and Notch Test (ISO 13479) are among the tests which are used to determine the resistance to slow crack propagation.

1.4. Characterization

A common structure in a semi-crystalline polymer contains very solid stacks of crystalline lamellae with non-crystalline regions between them. A HDPE with a narrow molecular weight distribution and small low molecular weight chains has a better impact resistance property. However, a wide molecular distribution makes the processing easier [3]. Using Ziegler catalyst, a bimodal weight distribution PE can be produced leading to a higher content of short chain branching in higher MW chains, higher environmental stress cracking resistance (ESCR), and superior processibilty [3, 7]. It is claimed that for newly developed plastics with bimodal molecular weight distribution claims, brittle failure and chemical degradation do not occur—even after 50-years of being in-service [3]. However, defining the knee position is still crucial to confirm the claims. In addition, developing a cost-saving accelerated testing method to predict the long-time performance of polymeric pipes depends on the understanding of their structure.

1.4.1. Effect of chain entanglements on brittle fracture

Entanglements between the molecular chains affect the crystallization and mechanical deformation of a polymer. There is a direct correlation between molecular weight, number of chain entanglements, and strain hardening behavior of a polymer in the range of moderate to high strains. As the network density of the amorphous region in a semi-crystalline polymer increases, the possibility of strain-induced disentanglement of the chains decreases because the network become stronger. In addition, the resistance to crack growth in polymers is correlated to the density of molecular links between the crystals including tie molecules and chain entanglements.

Different analytical methods including differential scanning calorimetry (DSC) [11], infrared spectroscopy (IR) [12], and solid state Nuclear Magnetic Resonance (NMR) [13-15] were used to understand the morphology of different semi-crystalline polymers. To understand the effect of the chain entanglements on molecular mobility, the spin-spin relaxation time T_2 should be measured which is smaller for entangled polymer chains compared with disentangled polymer chains [14, 15]. ^{1}H solid-state NMR was used for the

first time as the most sensitive method for measurements of molecular mobility changes to study the ductile failure of polymeric pipes at different temperatures under hydrostatic pressure test [14]. Perfection of the existing crystals, new crystal formation, and chain elongation in the amorphous phase due to creep under hydrostatic pressure were introduced as the causes of embrittlement of the samples [14]. Bimodal HDPE pipes show a significant improvement in slow crack growth (SCG) because of their composition of linear short chains and long chains with short side branches. As a result, ethylene short chains were used in some polymers such as random poly(polyethylene propylene) which may disturb the crystal formation and increase the creep resistance. The amount of the crystal phase is reported to be about 50% more than WAXD measurements as a result of small imperfect crystals and rigid crystal-amorphous interface [14]. The spin-spin relaxation time T_2 is sensitive to storage temperature and time. Sun et al. [15] have studied the morphology changes in unimodal and bimodal high density polyethylene pipes at elevated temperatures under hydrostatic pressure using ^{1}H solid-state NMR to understand their long term properties and structure-property relationships. The amount, thickness, and molecular mobility of the three introduced phases including crystalline phase, the interface (crystalline-amorphous), and amorphous phases were measured during the course of thermomechanical loading. The amount of crystalline region, the interlaminar spacing, and the molecular mobility of the amorphous phase are the most variable parameters during the course of storage time [15].

Cazenave et al. [16] studied the environmental stress crack resistance (ESCR) of high density polyethylene homopolymers and ethylene-hexane copolymers which are produced from three different synthesis methods using first and second generation chromium oxide catalysts and tandem-reactor Ziegler-Natta catalyst considering their molecular architecture. The chain topology and co-unit concentration and distribution on the molecular weight distribution are among the parameters which are examined on ESCR [16].

1.5. Existing models to predict creep rupture

Three types of models were used to predict the creep rupture of polymers [17]. One model considers the rupture as an activated rate process in which applied stress is related to time-to-failure by activation energy, activation volume, etc. The second model is a continuum

based model which uses mechanical dashpots and springs to model the relation. Finally, the last type uses experimental results, curve fitting, and extrapolation methods to predict the relation [17].

1.5.1. Creep rupture life estimation

There are number of techniques to predict the creep rupture life of PE pipes or the possibility of failure in 50 years. Barton and Cherry [18] modified the activated rate process equation developed by Eyring [19] and Coleman [20] to make the activation volume, temperature dependent. The modified equation can be used to predict the brittle creep rupture curve over range of temperatures. Because the ductile creep rupture curve could be measured by short term tests in room temperature, the intersection of the two curves was claimed to predict the creep rupture life (or the knee position).

$$\frac{dn}{dt} = \left(\frac{kT}{h}\right) \exp\left(\frac{-\varepsilon_0}{kT}\right) \exp\left(\frac{\beta\sigma}{2kT}\right)$$

where

$\frac{dn}{dt}$: the number of activated complexes passing over an energy barrier in unit time

σ: applied stress

β: activation volume for failure

ε_0: activation energy for failure

T: absolute temperature

h: Plank constant

k: Boltzmann constant

Based on the model, the failure stress was derived based on the time-to-failure and an assumed local critical failure strain,

$$\sigma = \frac{2kT}{\beta}\left(\ln N - \ln\frac{kT}{h} + \frac{\varepsilon_0}{kT}\right) - \frac{2kT}{\beta}\ln t_f$$

resulting in a simplified linear stress-log (time-to-failure) relationship with a slop of $\frac{2kT}{\beta}$.

Another (phenomenological) approach to predict creep rupture life was suggested by Sherby [21]

$$\dot{\varepsilon} = A\left[\frac{\sigma}{E(T)}\right]^n exp\ \left[\frac{-\varepsilon_0}{kT}\right]$$

in which $\dot{\varepsilon}$, $E(T)$, and n are strain rate, time dependent elastic modulus, and a constant respectively. If the same constant failure strain is assumed, a log (stress)-log (time-to-failure) relationship can be formulated

$$\ln \sigma = \frac{\varepsilon_0}{nkT} + \ln E(T) - n^{-1} \ln A + n^{-1} \ln t_f$$

where the equation was used to produce applied stress versus time-to-failure at different temperatures and then Arrhenius law was applied to relate the parallel lines, leading into time-temperature superposition. However, because of their different basis such as strain rate dependency of Arrhenius equation, the procedure failed to predict the creep rupture life time [18]. Furillo et al. [22] used Larson-Miller method, the Sherby equation, and the assumption of constant failure strain to make a new experimentally validated method.

$$\log \sigma = -\frac{1}{nT}\left\{T\left(\ln t_f - \ln\left[\frac{\varepsilon_f}{A}\exp\frac{\varepsilon_0}{kT}\right] - n \ln E(T)\right)\right\}$$

It was concluded [18] that by using both models, the brittle curves can be extracted. Therefore, using LTHS testing at higher stress and the produced curves, the transition knee from ductile to brittle curve is possible to be calculated.

1.5.2. Continuum based theories

Cherry and Teoh Swee Hin [17] used a combination of three-element model in combination of Reiner-Weissenberg thermodynamic energy failure theory [23] to predict the creep rupture of HDPE (Figure 1-3). In their study, the elastic response was divided to instantaneous and non-instantaneous recovery processes. To capture the whole response including the elastic and plastic, they used a Hookean storage element in series with a parallel arrangement of a dissipative element (Eyring dashpot [24]) and another Hookean storage element. Eyring dashpot is a non-Newtonian fluid based dashpot which its viscosity changes by a hyperbolic sine stress function. Reiner-Weissenberg thermodynamic energy failure theory assumes the failure happens when total of instantaneous and non-instantaneous elastic response reaches a critical value.

$$\int_0^{\varepsilon_a^*} \sigma_{re} d\varepsilon_a + \int_0^{\varepsilon_e^*} \sigma_{ap} d\varepsilon_e = R$$

where

ε_a^*: Anelastic strain at rupture

ε_e^*: Elastic strain at rupture

$\sigma_{re} = \varepsilon_a E_a$: Recovery stress

$\sigma_{ap} = \varepsilon_e^* E_e$: Applied stress

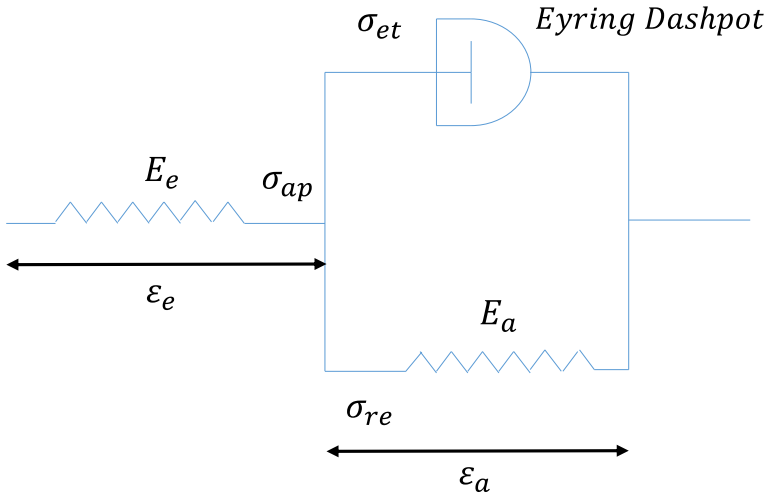

Figure 1-3. Three-element model to predict creep rupture [17]

By considering σ_{ap} as a constant under creep and solving the equation

$$\varepsilon_a^* = \left[\frac{2}{E_a}\left(R - \frac{\sigma_{ap}^2}{E_e}\right)\right]^{1/2}$$

Based on Reiner-Weissenberg thermodynamic energy failure theory, anelastic strain is predicted as follows

$$\dot{\epsilon}_a = K \sinh(\beta \sigma_{ef})$$

in which K and β are a function of activation energy and activation volume, repectively.

1.5.3. Time-Temperature-Stress superposition technique

The magnitude of the applied stress and physical aging can influence the creep response of high density polyethylene (HDPE). In fact the short creep data from [25] shows relaxation time distribution can be shifted even by low stress levels. However, at low stress, the aging rate is independent of stress because of strong material nonlinearity. One of widely used methods to fit creep data is Kohlrausch-Williams-Watts (KWW) relation

$$D(t) = D_0 \exp[(t/t_0)^\gamma]$$

in which t_0 is a temperature and aging time dependent value called the mean relaxation time and D_0 and γ are fitting constants. However, this relation is only valid at the start of α relaxation. The other valid method to predict the creep compliance over longer period of time is the so-called time-temperature superposition principle. This can model the shift in relaxation time distribution by a change in temperature because of temperature-induced free volume change. The compliance at two different temperatures T_0 and T_1 are related as follows

$$D(t, T_1) = D(t/a_T, T_0)$$

The time-temperature shift factor, a_T, can be obtained by Williams-Landel-Ferry (WLF) equation

$$\log a_T = \frac{C_1(T - T_g)}{C_2 + (T - T_g)}$$

where T_g, C_1, and C_2 are the glass transition temperature and two fitting constants, respectively. Strictly speaking, the equation is only valid for thermo-rheologically simple polymers such as amorphous polymers. However, the response of a semi-crystalline polymer is more complex.

The other concern for modeling the creep compliance using time-temperature superposition is physical aging. Physical aging is the slow and gradual process of the polymer reaching an equilibrium configuration at temperatures below T_g because of slow molecular mobility. During physical aging, the material becomes more brittle and stiffer, decreasing the creep and relaxation rates because of free volume reduction. Time-temperature superposition can only describe the short-time creep behavior in which the creep time is shorter than time for physical aging. As a result, for longer creep response, physical aging effect should be included in the modeling using techniques which were employed by Gates et al. [26].

The time-temperature superposition principle can only be used for HDPE if the effect of applied stress and physical aging are considered. At room temperature, there are three phases present in the HDPE structure including: (1) the amorphous region, which is more mobile above its T_g and which has a non-linear behavior under low stress as a result of increased free volume (2) the amorphous-crystalline region, which acts as glassy amorphous

region below its glass transition with a linear behavior, and (3) the crystalline region, which also contributes to the elastic deformation. Therefore, Lai and Bakker [25] used a combination of horizontal and vertical shifts to produce the master curve of creep compliance using time-stress superposition. To consider the effect of physical aging, they performed a series of short time creep tests with different elapsed physical aging times in different low stress levels. As a result, a time-aging superposition was formed using horizontal and vertical shifts because of amorphous-crystalline region and amorphous regions, respectively. The horizontal shift factor was used to incorporate the aging effect in long-term creep expression.

1.5.4. Ree-Eyring model

Relaxation processes in semi-crystalline polymers have dominant effects on their physical properties. For example, they cause stiffness or modulus to change in specific regions. In general, 3 relaxation processes in semi-crystalline region include: (1) α relaxation which molecular motions in the crystalline phase are responsible for it (if the process is assigned by NMR and dielectric measurements. However, in the case of mechanical response, their effect is conveyed with both phases). In fact, a combination of redistribution of the loose and tight chain, cilia, and inter-crystalline links affected by crystalline phase confinement and chain diffusion between crystalline and amorphous phases cause α relaxation [27] (2) β relaxation which is associated to amorphous phase of polymer, and (3) γ relaxation which happens in very low temperatures. Both α and β relaxation processes depend on the crystal thickness [28, 29].

To understand the nature of yielding in semi-crystalline polymers, Seguela et al. [30, 31] studied the plastic behavior of polyethylene and ethylene copolymers under uniaxial tensile testing. It was observed that if the temperature of the experiment is higher than the α relaxation temperature, a semi-crystalline polymer usually shows additional plastic behavior (or yielding) in the true-stress/true-strain curve which is called homogenous plastic deformation [31]. In addition, the homogenous crystal slip is likely to cause plastic deformation if the applied strain rate is affordable by the rate of nucleation and propagation of screw dislocations. The thermally activated process is as a result of nucleation and propagation of shear deformation because of 180° twist [32] and half unit translation of

crystalline stems [28, 29] (Figure 1-4). The twisting is transferred from one stem to its neighbor until the dislocation line completes (Figure 1-4) or the motion is prevented because of tight folds. The dislocation finally escapes from the plane opposite to the plane which it was started. In fact, the behavior is in direct relation to the crystal lamella thickness and molecular mobility of the crystalline chains. The α relaxation temperature decreases with decreasing crystal thickness which happens when co-unit concentration increases in copolymers [31]. The dislocation is also able to be activated at lower temperatures if the crystal thickness decreases because it needs smaller thermal activation to migrate through the whole crystal. Thus, co-polymers with less crystallinity possess thin crystals and lower α relaxation temperature. The tensile strain-induced crystal thickness increase (the mechanically assisted annealing effect during tensile drawing) also participates in the crystalline α relaxation if the drawing temperature is close or above α relaxation temperature.

In case of low temperature (below the α relaxation temperature) or high strain rate experiments, the dislocation becomes inhibited because of tight lamellae (topological restrictions). If the drawing temperature decreases, the chain defect transformation becomes very slow which cannot be afforded by the strain rate of the experiment. Therefore, crystalline defects generated by a critical shear stress, co-unit side groups, or stress concentrations may nucleate a localized slip and thus a macroscopically heterogeneous plastic instability. The localized heterogeneous slip is unstable and causes the lamellae fragmentation parallel to the draw direction even without thermal activated nucleation [30].

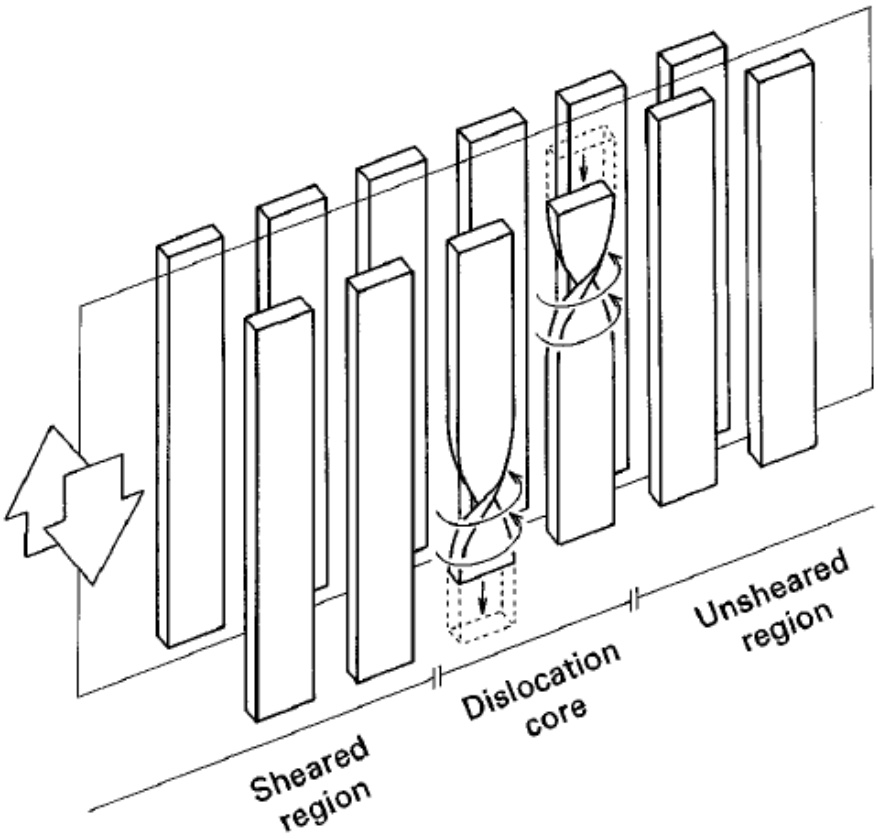

Figure 1-4. Screw dislocation propagation in idealized ribbon-like crystalline stems [31]

Butler et al. [33] defined the macroscopic tensile yield point as a result of onset of crystalline orientation, decrease in the equatorial long spacing (because of lamellar thinning), activation of the martensitic transformation (resulting in the conversion of orthorhombic into monoclinic material), and onset of cavitation (crystallographic deformation when the inter-lamellar regions were unable to withstand the applied strain) based on small angle X-ray scattering and wide angle X-ray diffraction (SAXS and WAXD) measurements. However, cavitation was not observed in compressive yielding [34].

Understanding of the two processes and the modified Eyring model by Bauwens-Crowmodified et al. were the foundation to predict the long-term behavior of microscopically heterogeneous semi-crystalline polymers based on their short-term behavior (yield stress which is strain and temperature dependent) [27, 35]. At the beginning of the modeling attempts, instead of considering a single crystallographic slip which was proposed by Bowden-Young [36] and Seguela et al. [30, 31], refined slip kinetics were used to model texture evolution. The micromechanically based constitutive model [37, 38] was

modified in a series of papers by Van Dommelen et al. [27, 35, 39] to explain the complex double yielding kinetics of semi-crystalline polymers including HDPE. The model considers the semi-crystalline polymer as an aggregate of two-phase layered composite inclusions in which (1) amorphous phase was considered to be isotropic elasto-viscoplastic influenced by the crystalline region and (2) crystalline lamellae was modeled as an anisotropic elastic material with plastic flow because of crystallographic slip. The two phase were coupled by kinematical compatibility and traction equilibrium. The shear rate of both phases was related to shear stress by a modified Ree-Eyring flow theory (the theory was originally developed to describe the relaxation processes of viscous flows for liquids). However, the proposed model did not mean to identify any coarse slip (crystal fragmentation) proposed by Butler et al. [33, 34] which happens experimentally at the second yield. As the result of the modeling process, the crystallographic slip in the amorphous region, (100)[001] chain slip, and a combination of (100)[010] and $\{110\}\langle 1\bar{1}0\rangle$ transverse slip systems were recognized as the reason for the first and the second yielding, respectively. In addition, the yield stress dependence to temperature and strain rate for polyethylene was decomposed into the two explained parallel molecular processes [4] which are due to (1) intralamellar deformation because of crystal slip [30, 31] at higher temperatures and low strain rates and (2) α-transition (interlamellar deformation) [28].

Because of the possible occurrence of both homogenous and heterogeneous slip processes and the effect of hydrostatic pressure [40], Bauwens-Crowet in a series of studies [41-44] showed that the yield behavior (tensile and compressive) dependence of several polymers to temperature and strain rate is possible to be modeled by two Eyring processes in parallel, $\sigma_y = \sigma_1 + \sigma_2$, (1) low pressure, high temperature, or low strain rates (2) high pressure, low temperature, or high strain rates conditions in which σ_1 and σ_2 represent the flow stresses for processes 1 and 2, respectively.

1.5.1. Accelerated creep characterization technique

Recently a new experimental approach was proposed that is able to predict the plasticity-controlled failure (ductile failure) of HDPE pipes within a few weeks of testing [4] using the pressure modified Eyring flow equation. Uniaxial tensile tests were used to determine the yield strength variations based on strain rate changes in different temperatures. To account

for pressure dependence of the response, uniaxial compression tests were also conducted. The Ree-Eyring modification of pressure-modified Eyring flow condition in addition to assumption of existing a critical amount of accumulated plastic strain for failure is employed to capture plastic flow kinetics and prediction of time-to-failure [4].

In the approach, the creep response of solid polymers includes three regions (**Error! Reference source not found.**): after an initial elastic response: the strain rate (1) decreases (primary creep) (2) approximately remains constant ($\dot{\varepsilon}_{pl}$) (secondary creep) (3) and then increases (tertiary creep) resulting in plastic strain localization and final failure. An increase in stress or temperature will accelerate the process and reduce the time-to-failure.

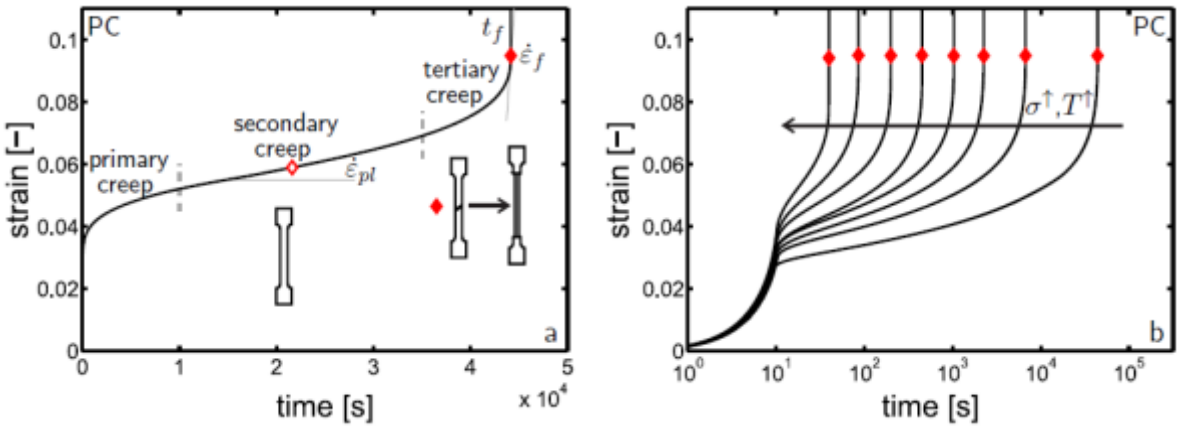

Figure 1-5. (a) 3 regions of creep response for polymers (b) temperature and stress dependent response of polymers [4]

Crissman and McKenna showed the time to failure t_f, multiplied by the strain rate at failure $\dot{\varepsilon}_f$ is constant in creep rupture of polymers for different stresses [45]

$$\dot{\varepsilon}_f(\sigma).t_f(\sigma) = C_1 \quad or \quad \frac{\dot{\varepsilon}_f(\sigma_1)}{\dot{\varepsilon}_f(\sigma_2)} = \frac{t_f(\sigma_1)}{t_f(\sigma_2)}$$

Mindel and Brown also demonstrated that for polycarbonate the stress dependence of flow is independent of strain which helps to relate the strain rate at failure to flow rates during the secondary creep $\dot{\varepsilon}_{pl}$. As a result

$$\dot{\varepsilon}_{pl}(\sigma).t_f(\sigma) = C_2$$

The constant C_2 was considered to be the accumulated plastic strain for its life to failure under a constant load as a critical strain, ε_{cr}. Therefore, creep rupture life can be predicted

if the stress and temperature dependence of the plastic flow rate (the second creep region slope) and the critical strain are known [45]

$$t_f(\sigma, T) = \frac{\varepsilon_{cr}}{\dot{\varepsilon}_{pl}(\sigma, T)}$$

Instead of conducting a time-consuming creep test (especially at very low stresses or low temperatures), a constant strain rate test can be used to accelerate the time to failure prediction. It was demonstrated [44] that for polycarbonate, the secondary creep region is identical to the condition of yielding region in a constant strain rate test.

To predict the stress and temperature dependence of the plastic flow rate, a pressure modified Eyring activated flow relation [46] developed by Ward [47] was used by Kanters [4]

$$\dot{\bar{\varepsilon}}_{pl}(\bar{\sigma}, T) = \dot{\varepsilon}_0 \exp\left(-\frac{\Delta U}{RT}\right) \sinh\left(\frac{\bar{\sigma} V^*}{kT}\right) \exp\left(-\frac{\mu p V^*}{kT}\right)$$

$\bar{\sigma}$: Equivalent von Misses stress

$\dot{\bar{\varepsilon}}$: Equivalent von Misses strain rate

$\dot{\bar{\varepsilon}}_{pl}(\bar{\sigma}, T)$: Stress and temperature dependent equivalent plastic flow rate

$\dot{\varepsilon}_0$: A constant strain rate which depends on age and crystallinity of material

T: Absolute temperature

ΔU: Activation energy

V^*: Activation volume

R: Universal gas constant

k: Boltzmann's constant

p: Hydrostatic pressure

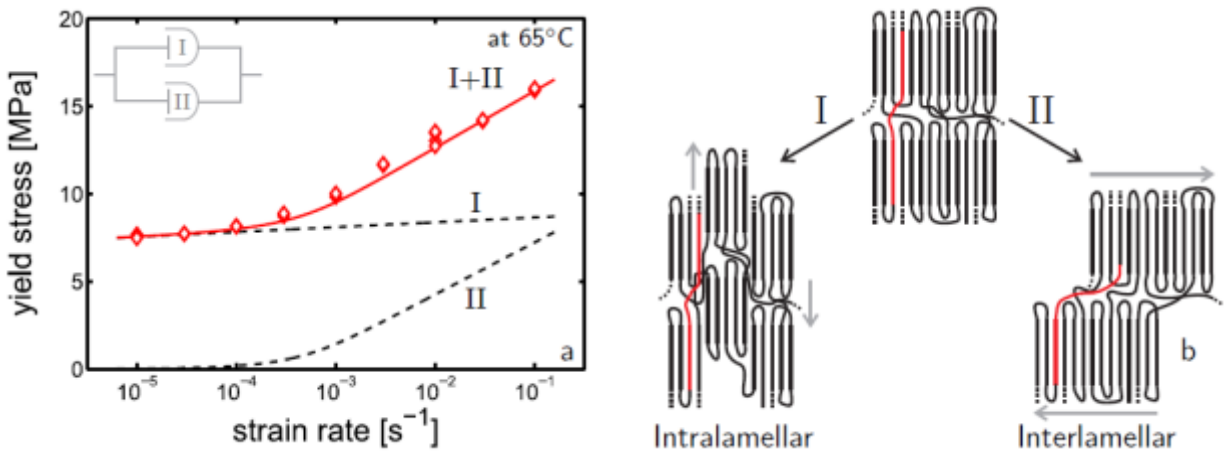

Figure 1-6. two parallel process which described by Ree-Eyring [48] and Kanters [4]

Using the model and the fact that creep response is a combination of two parallel molecular processes, and the effect of hydrostatic pressure is similar for both processes, Ree and Eyring [48] proposed a model to predict the rate dependence of the system

$$\bar{\sigma}\left(\dot{\bar{\varepsilon}}_{pl},T\right)=\bar{\sigma}_I\left(\dot{\bar{\varepsilon}}_{pl},T\right)+\bar{\sigma}_{II}\left(\dot{\bar{\varepsilon}}_{pl},T\right)=\frac{kT}{V_I^*}\sinh^{-1}\left(\frac{\dot{\bar{\varepsilon}}_{pl}}{\dot{\varepsilon}_{0,I}}\exp\left(\frac{\Delta U_I}{RT}\right)\right)+\frac{kT}{V_{II}^*}\sinh^{-1}\left(\frac{\dot{\bar{\varepsilon}}_{pl}}{\dot{\varepsilon}_{0,II}}\exp\left(\frac{\Delta U_{II}}{RT}\right)\right)+$$

$$\mu p$$

μ is a pressure dependent constant that needs to be determined by a tensile test superimposed by an external hydrostatic pressure on a polymer [4, 49, 50]. However, Kanters proposed a combination of uniaxial tensile and compression testing [4] and the resulting yield stresses to calculate the constant

$$\mu = 3\times\frac{\bar{\sigma}_c-\bar{\sigma}_t}{\bar{\sigma}_c+\bar{\sigma}_t}$$

In which $\bar{\sigma}_t$ and $\bar{\sigma}_c$ are equivalent von Mises yielding stresses under tensile and compression loading, respectively. Subsequently, constant stress (creep) experiments were employed to calculate the critical strain [4]. Therefore, combination of Ree-Eyring model and creep tests (used to calculate the critical strain) is able to predict the time-to-failure based on the applied stress.

As a result of pipe extrusion, residual stresses can be introduced when the melt is cooled down. The outside wall freezes in contact with water but the internal wall is still hot. Hence, the inside material wants to expand but the frozen outer layer hinders the expansion. This process presents tensile residual stress inside and compressive residual stress outside. However, the residual stresses are able to relax by annealing at 80°C or over a long period of

time in reference temperature. In order to capture the influence of processing conditions in the form of residual stresses, the samples used by Kanters [4] for tensile and compression testing were compression molded in a hot-press in different cooling rates. However, the state of residual stress (because of temperature history) measured for an extruded pipe is very complex, not uniform, and different for different dies and materials [3]. In this study, to consider the effect of processing condition, a testing procedure is presented that uses the samples which are cut from the actual SDR 11 pipes rather than compression molded samples.

Chapter 2

2. Experimental procedure

2.1. Materials

All pipes were provided by LyondellBasell Industries (Cincinnati Technology Center, OH). Four different SDR 11 pipe configurations were produced from (1) LB1 resin melted at 389 °C using an Old Die/Standard Sleeve; (2) LB2 resin melted at 387 °C temperature using an Old Die/Standard Sleeve; (3) LB1 resin melted in 389 °C temperature using a New Die/ISO Sleeve; and (4) LB2 resin melted in 387 °C temperature using a New Die/ISO Sleeve. After extrusion, all the pipes were cooled down in a water tank with the temperature of 24-26 °C. Henceforward, the configurations will be called ODLB1, ODLB2, NDLB1, and NDLB2, respectively.

2.2. Fixture and test Design

To include the effect of processing state (i.e. inherent manufacturing conditions including the defects, non-uniform thickness, non-uniform residual stresses, etc.), a new procedure is proposed for tensile testing. A threaded fixture (Figure 2-1) was designed for SDR 11 pipes. The fixture was screwed in the samples which were cut from the actual pipes having the gauge length of 100 mm. To decrease the effect of stress concentration on the pipes (and the possibility of failure) because of the sharp edges of the thread, the fixture was cut with a very slight angle from the top. As a result, no sharp edge was present on the thread at the start of the gage length on both sides. Subsequently, the samples were speckled with non-flammable white color paint to make a high contrast pattern and facilitate Digital Image Correlation (DIC) measurements of the pipes deformations. Two STBC131 T hose clamps from Thaman Rubber Co. (Cincinnati, OH) were used on each side to fix the pipes on the fixture (Figure 2-2). A torque-meter was also used to apply 90 lb.in torque on the hose clamps. The same fixture was used to conduct the tensile creep testing on the pipes as well.

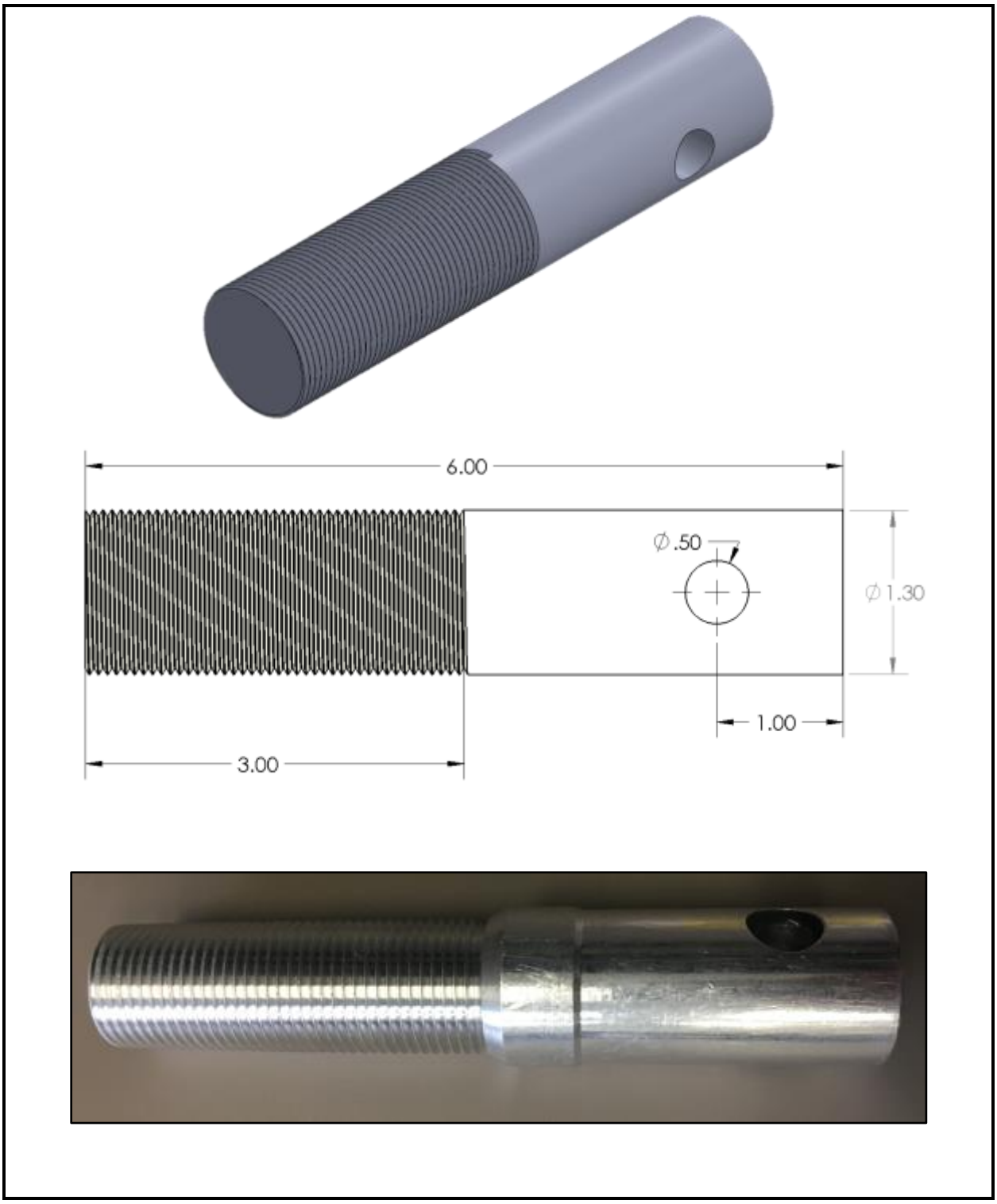

Figure 2-1. A threaded fixture designed for tensile testing on the actual pipes (dimensions are based on inches)

In addition to the tensile characterization, compression tests are also necessary to complete the approach of Kanter. The known problems with compression testing are global buckling, wrinkling, barreling, etc. and it is very hard to avoid two latter problems. Therefore, for the compression testing on the actual pipes, four different sizes of the pipe were cut with L/D of 0.6, 0.8, 1, and 1.2. The compression samples were tested using custom compression platens.

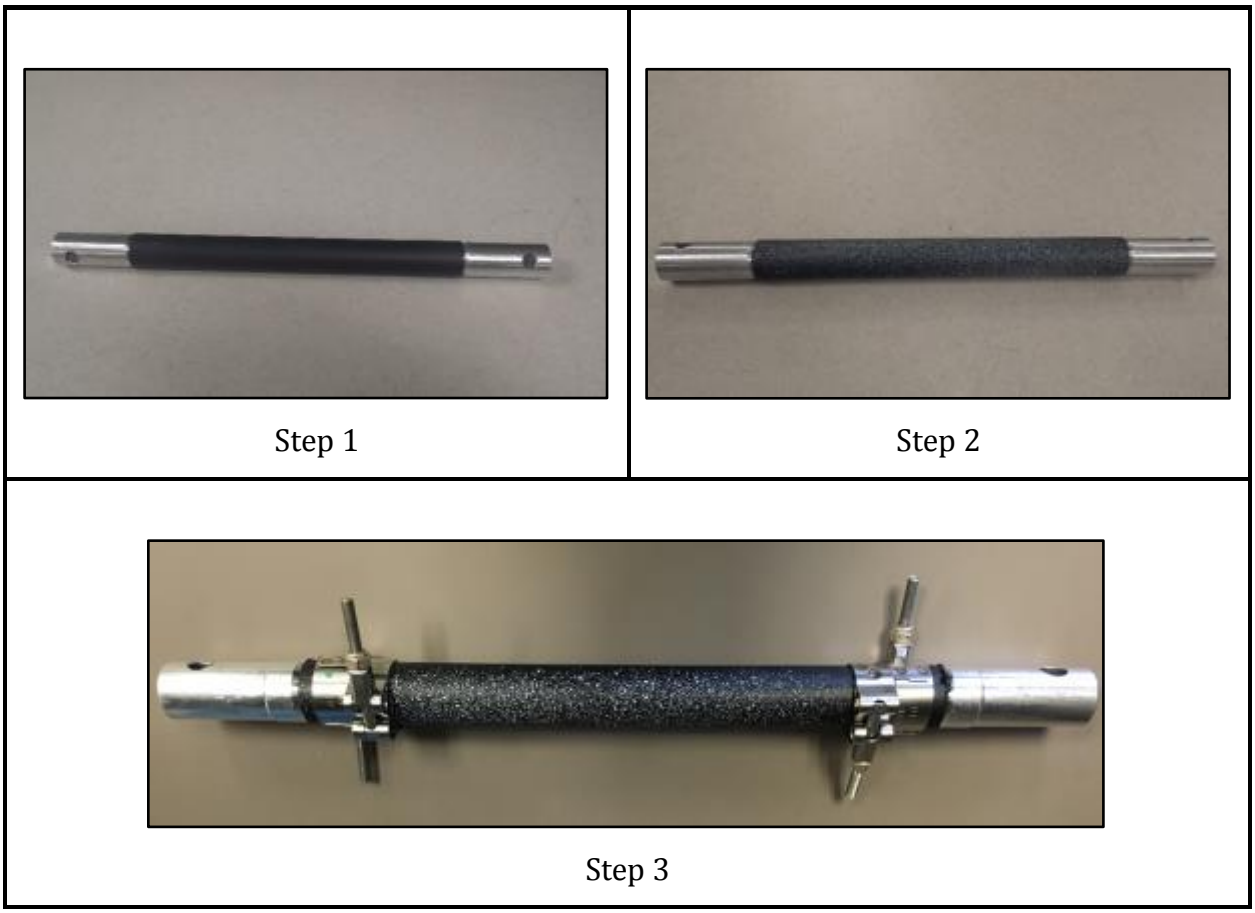

Figure 2-2.Tensile sample preparation includes (1) screwing the threaded fixture into actual pipe (2) speckling the sample around the gage length (3) fixing the pipe on the fixture using the hose clamps

To test the actual pipes under hydrostatic pressure, a fixture was designed based on the ISO 1167 standard which includes two different geometries (1) One with end caps connected to one another using a metal rod in which the internal hydrostatic pressure resulted in hoop stress alone (Figure 2-3) (2) One in which end caps were connected to the samples with hose clamps led to axial and hoop stresses (the fixture used by LyondellBasell).

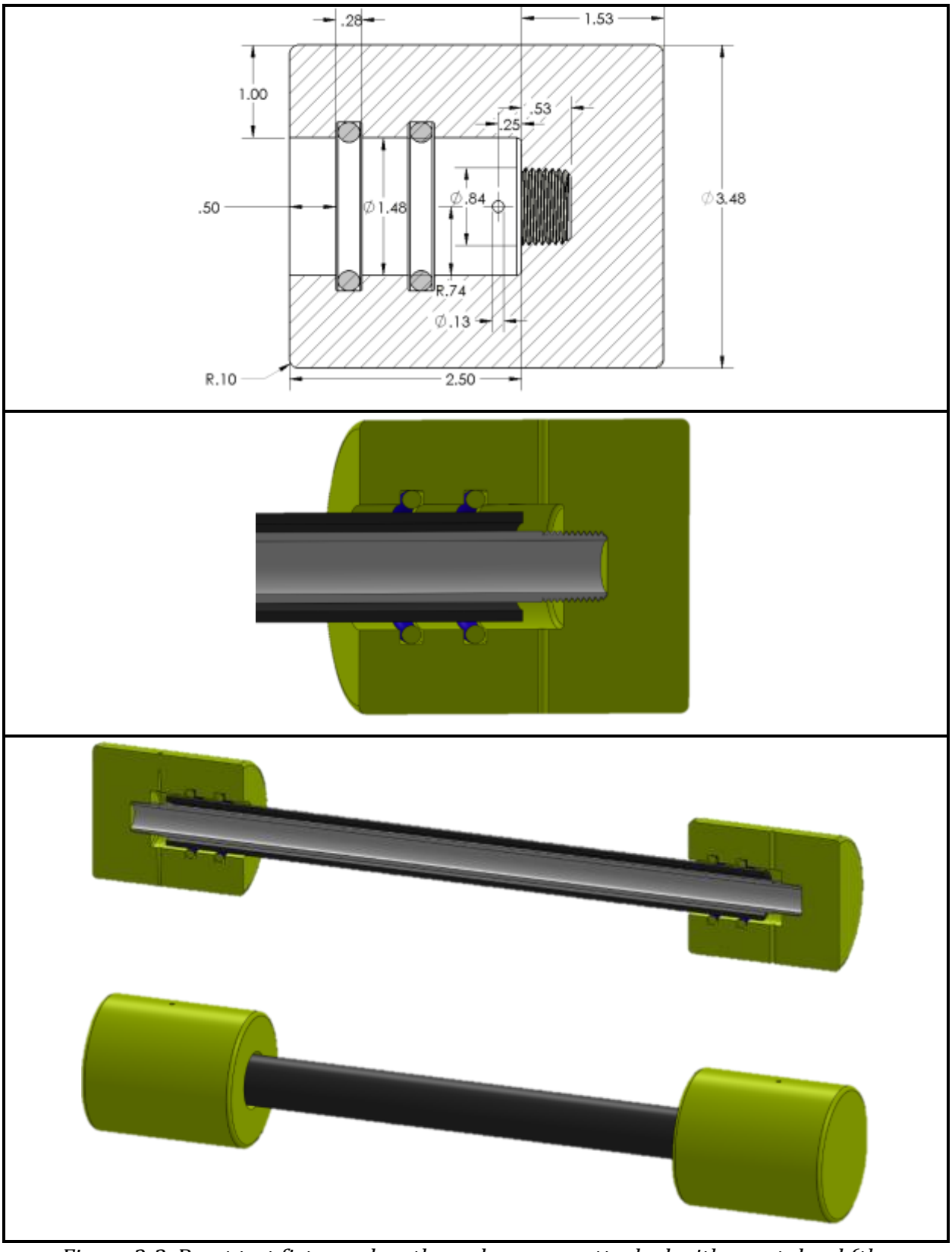

Figure 2-3. Burst test fixture when the end caps are attached with a metal rod (the dimensions are based on inches)

2.3. Mechanical testing

Compression and tensile yield strength of the pipes were measured using a screw-driven Instron load frame with a 50 kN load cell (Figure 2-4). Each configuration was tested in three different strain rates and under 4 different temperatures including room temperature (23°C), 40°C, 60°C, and 80°C. Tensile testing measurements were repeated 3 times. Because of very low standard deviation of the tensile testing results, it was decided to repeat the compression tests only two times. The strain was measured using two methods: (1) an MTS 634, 11E-54 extensometer and (2) using the Digital Image Correlation (DIC) technique for a single sample. DIC equipped with Aramis software v6 developed by GOM was used to ensure there is no misalignment in the samples. In addition to show that the specified strain rate is consistent with the observed strain rate, and that the strains are uniform within the gage length. Hence, two megapixel cameras were used to have in-plane strain on the pipe cylindrical surface. The DIC system was calibrated at the beginning. The average intersection deviation error of all 3D points was less than the maximum recommended value of 0.3 [51]. Number of images in each measurement was adjusted based on the strain rate. Subsequently, the strain in x and y directions were determined using the captured images in which each image taken by cameras was divided by square facets with a size of 23-pixels and a facet distance of 15-pixels.

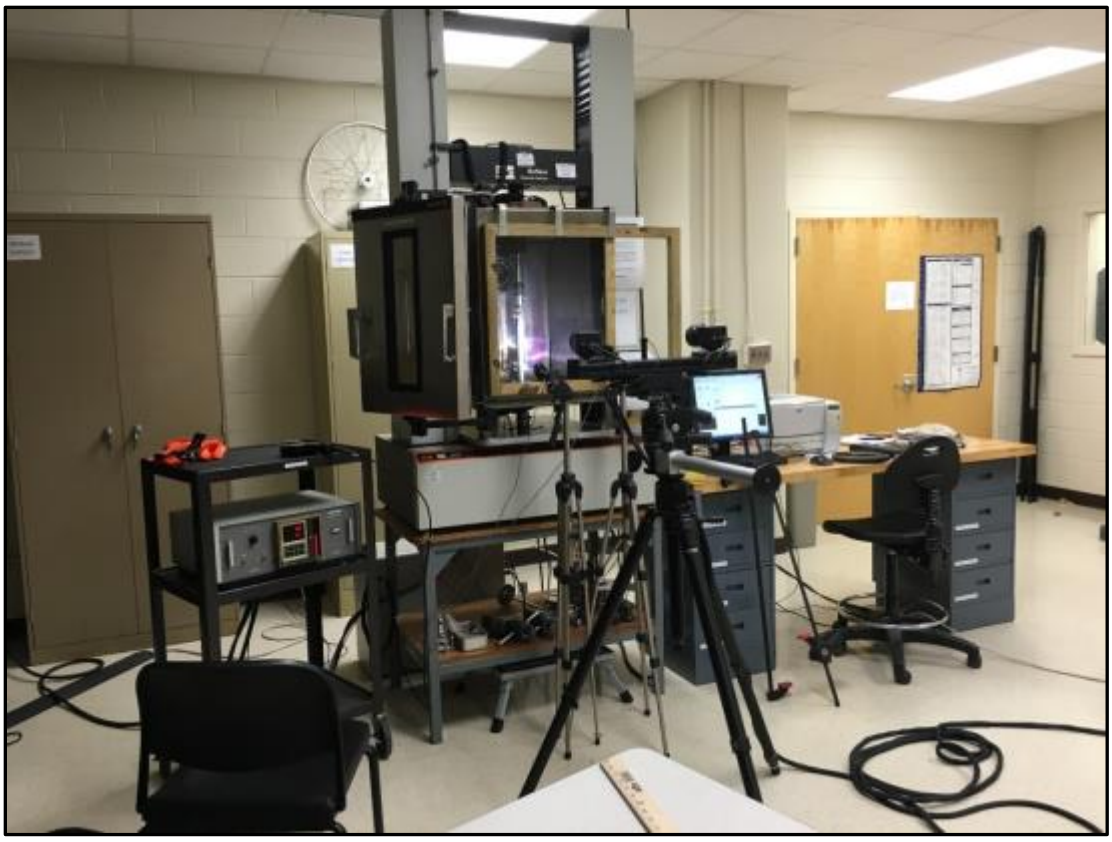

Figure 2-4. Screw-driven Instron frame with 50 kN load cell and oven when DIC measurements were done

To conduct hydrostatic pressure tests, the samples were first cut into 254 mm sections, speckled with white paint, and placed between end caps supplied by LyondellBassel fixture. Water was pumped inside the pipe. Once the sample and reservoir were filled with water, the pump was stopped. Subsequently, compressed nitrogen (N_2) gas was charged into the reservoir and using the pressure transducer, the internal pressure of each pipe section was kept constant. Figure 2-5 shows a schematic of the setup and the actual system. To measure the strains in axial and hoop directions, DIC was used. Images taken by cameras were divided into square facets with a size of 23-pixels and a facet distance of 15-pixels; the imaging rate was adjusted based on the time of experiments. Each test was repeated at least two times to make ensure consistent results. Finally, the time-average of pressure and the time to failure was reported for each experiment.

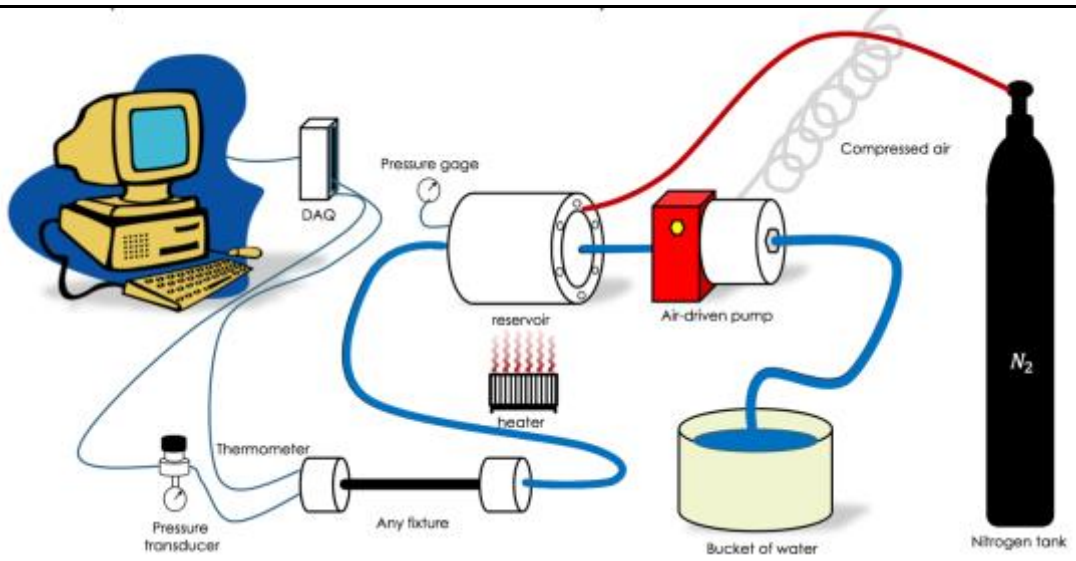
DAQ
Pressure gage
Compressed air
reservoir
Air-driven pump
N_2
heater
Thermometer
Pressure transducer
Any fixture
Bucket of water
Nitrogen tank

(a)

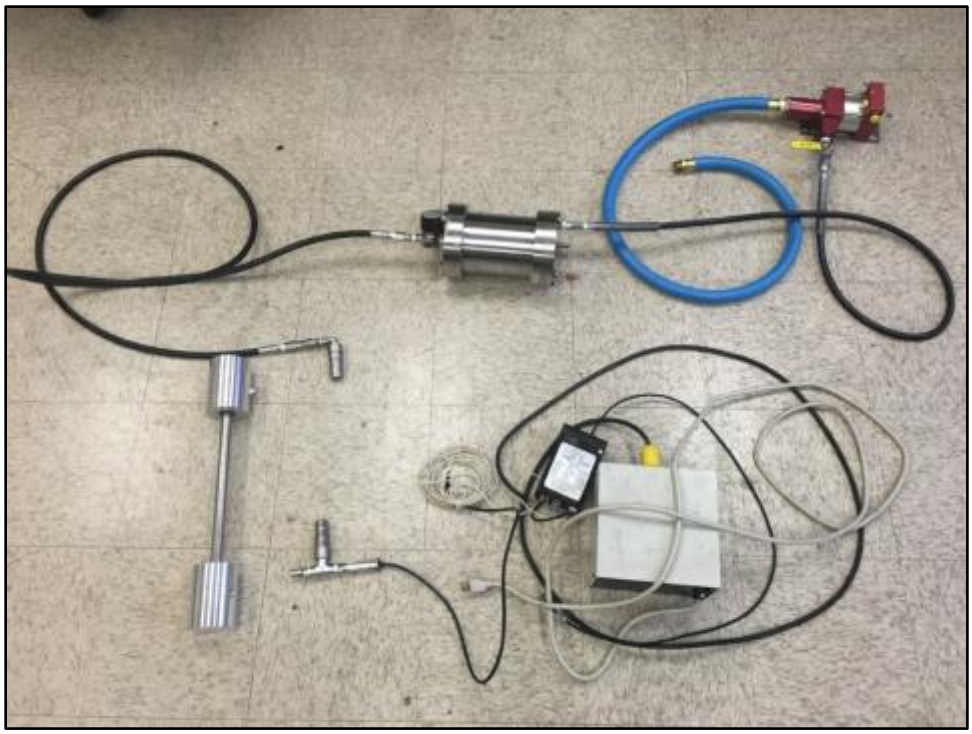

(b)

(c)

Figure 2-5. (a) Schematic of the burst test set-up, (b) the actual set-up, and (c) ductile failure of a PE pipe section using the LyondellBasell LTHS fixture

2.4. Pipe characterization using SAXS/WAXD

SAXS experiments were performed using a Rigaku S-Max 3000 3 pinhole SAXS system, equipped with a rotating anode emitting X-ray with a wavelength of 0.154 nm (Cu Kα). The sample-to-detector distance was 1605 mm, and the q-range was calibrated using a silver behenate standard. Two-dimensional SAXS patterns were obtained using a fully integrated 2D multiwire, proportional counting, gas-filled detector with an exposure time of 2 h. All SAXS data were analyzed using the SAXSGUI software package to obtain radially integrated SAXS intensity versus scattering vector q, where $q = \left(\frac{4\pi}{\lambda}\right) sin(\theta)$, θ is one half of the scattering angle, and λ is the wavelength of X-ray.

WAXD were performed using a Rigaku MiniFlex II x-ray diffractometer emitting X-rays with a wavelength of 0.154 nm (Cu Kα). Samples were scanned from 5 to 35° 2θ at a scan rate of 0.25° 2θ/min and a sampling window of 0.050 2θ at a potential of 30 kV and current of 15 mA. All WAXD data were analyzed using the PDXL 2 software package to obtain WAXD

intensity versus 2θ profiles, where θ is one half of the scattering angle. WAXD profiles were vertically shifted to facilitate a comparison of the peak positions.

Chapter 3

3. Results

3.1. Morphology characterization

SAXS was used to study the three-dimensional morphological arrangement of crystallites formed during processing of the SDR 11 pipes. NDLB1 or ODLB1 pipes were chosen as examples of having the same material (LB1) which were produced by new and old dies. The resulting spectrum, Figure 3-2, show that the peak positions do not significantly change, which indicates that the inter-crystallite distance is also constant. All of the pipes analyzed were uniform when considering the hoop and axial directions of the pipe. No measurable anisotropy exists for either NDLB1 or ODLB1 in either SAXS or WAXD. This is indicated by the fact that the 2D intensity distribution is constant with respect to angle when measuring SAXS through the thickness. The ODLB1, in fact, shows the highest degree of anisotropic behavior going through the thickness of the pipe. Figure 3-1 shows a typical 2D WAXD pattern for mentioned samples, as can be seen the rings present appear to be equal in intensity in all directions, which indicates an isotropic distribution of crystalline lattice planes within the material.

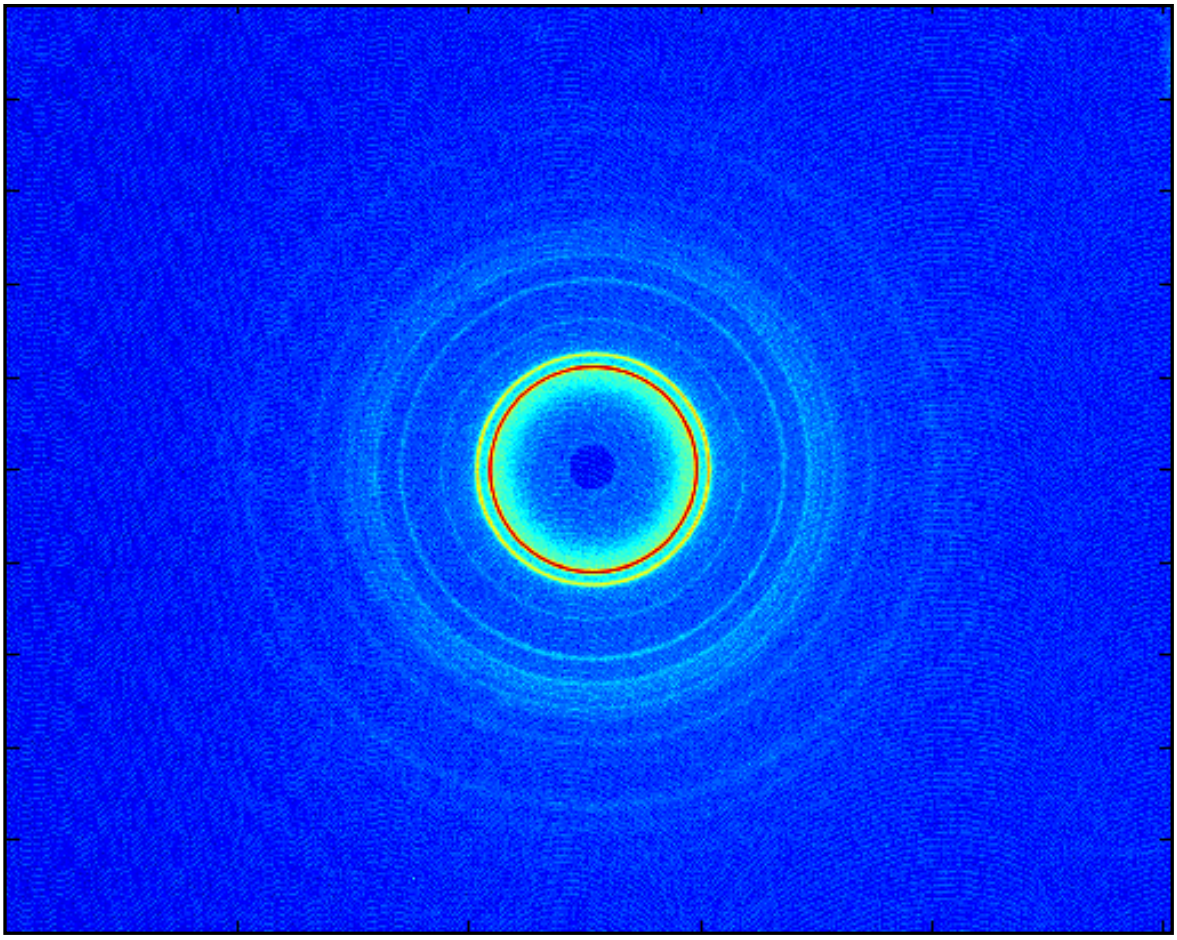

Figure 3-1. 2D WAXD pattern of NDLB1inner layer

In order to compare the distribution of crystallites in the material through the thickness three different layers have been cut from the pipes. The samples representing each layer was in square shape with the side size 10 mm and thickness of 0.5 mm. When comparing both NDLB1 and ODLB1 inner, middle, and outer layers, Figure 3-2 and Figure 3-3 demonstrate that the layers are nearly isotropic. However, the average Bragg spacing, (inter-crystallite spacing (d)) increases from inside to outside. The increase in the Bragg spacing (d) is < 5% of the total distance and can be expected to exhibit isotropic properties throughout the thickness.

WAXD data was also taken on the same samples in order to compare the total crystallinity and investigate possible differences in the crystal structure. The total crystallinity can be computed as a ratio of the area of crystalline peaks and the total area under the curve. As the same as the SAXS data, Figures 3-4 and 3-5 show that there are small differences in the layers,

however these differences in the total crystallinity are small compared to total crystallinity. The differences in each layer again are <5% in respect to crystallinity.

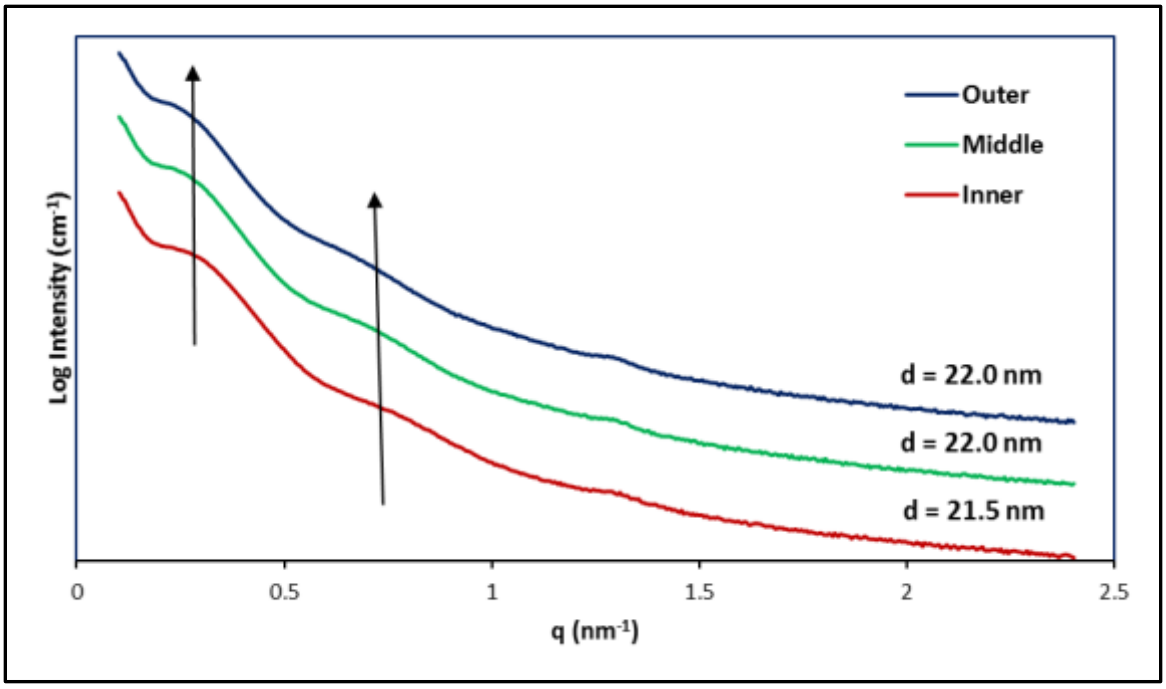

Figure 3-2. 1D SAXS profiles of NDLB1

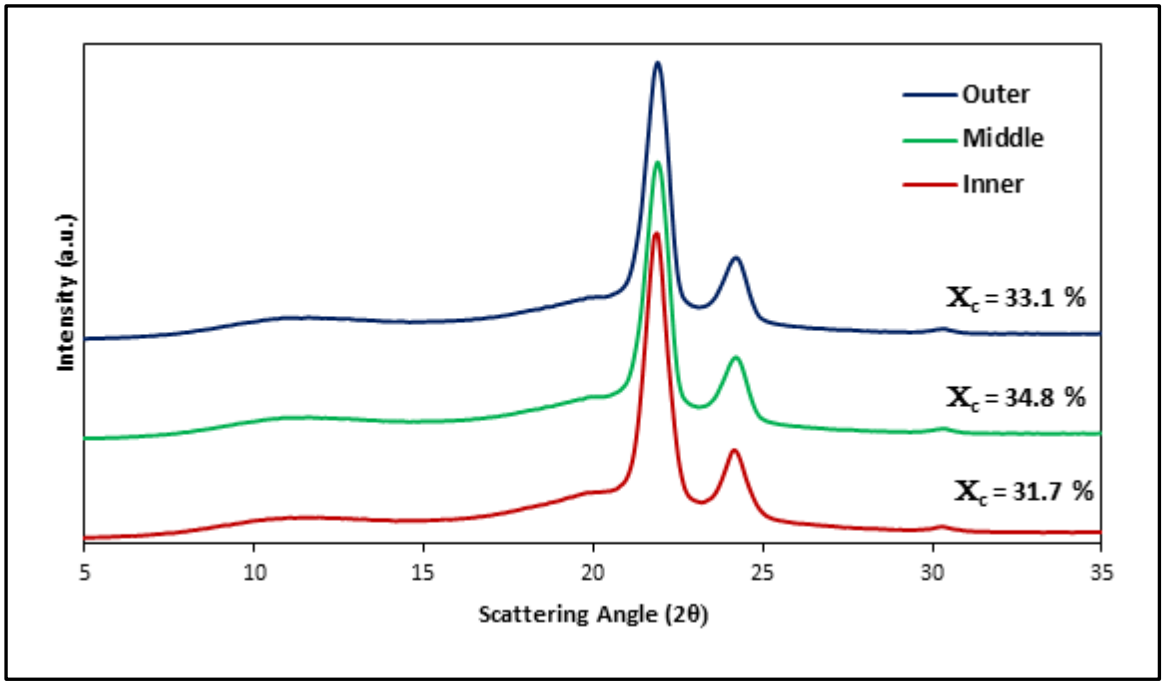

Figure 3-3. WAXD profiles of NDLB1

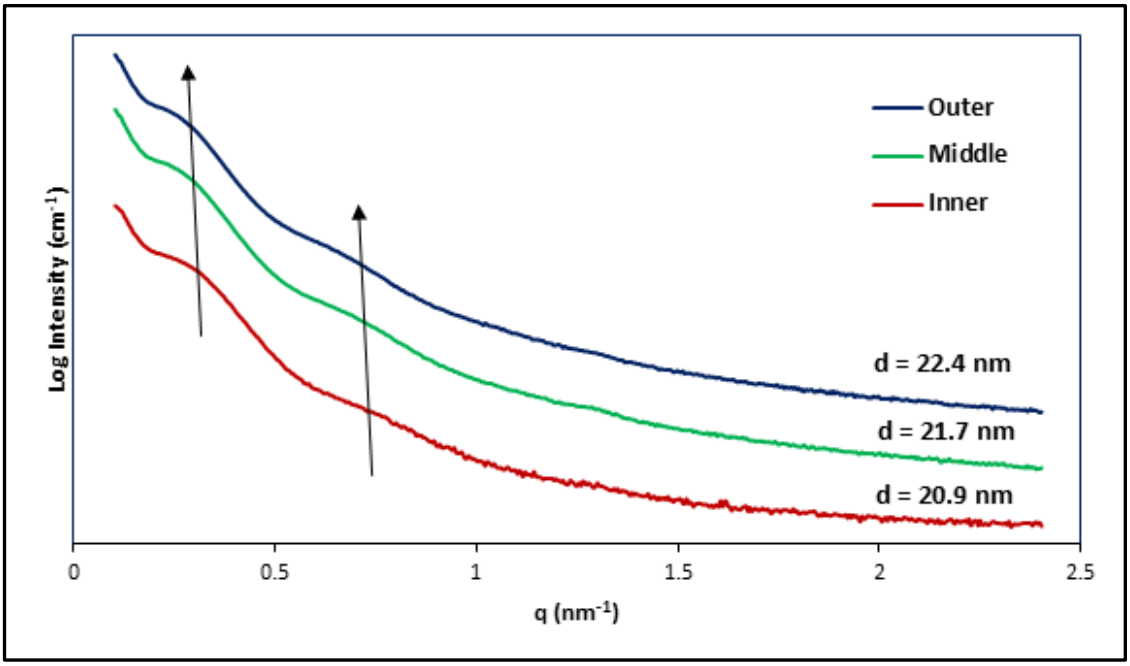

Figure 3-4. 1D SAXS profiles of ODLB1

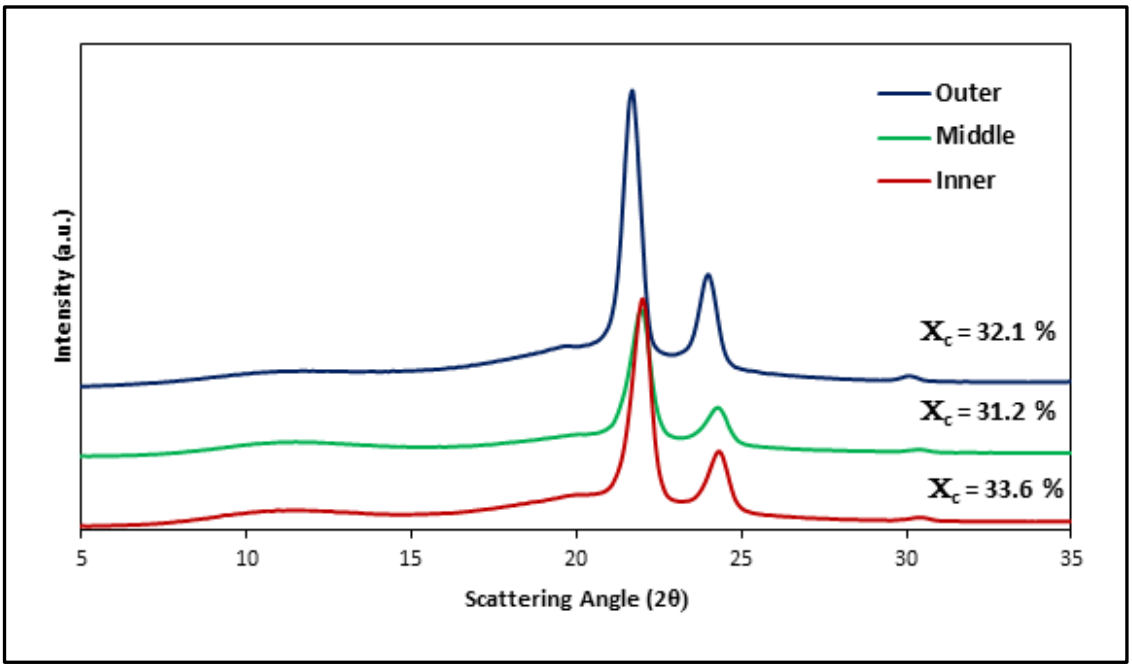

Figure 3-5. WAXD profiles of ODLB1

3.2. Mechanical characterization

Figure 3-6 shows stress-strain data for a tensile test obtained using DIC and an extensometer for a preliminary HDPE sample produced by LyondellBasell Industrial Co. There is not a significant difference between the stress-strain results measured using the techniques. Figure 3-7 illustrates the uniformity of the strains within the gage section based on the DIC results. Furthermore, an advantage of using DIC technique is the ability to measure strain results in each point between screws even at each end. Figure 3-8 shows LB1 pipe (SDR 11) which was tested at a rate of 10 mm/min at 40°C. Three 3D points within the gage length were chosen representing: (1) upper (2) middle, and (3) lower parts of the 100 mm gage length. The results shown here serve to further reinforce the uniformity of the strains within the gage section.

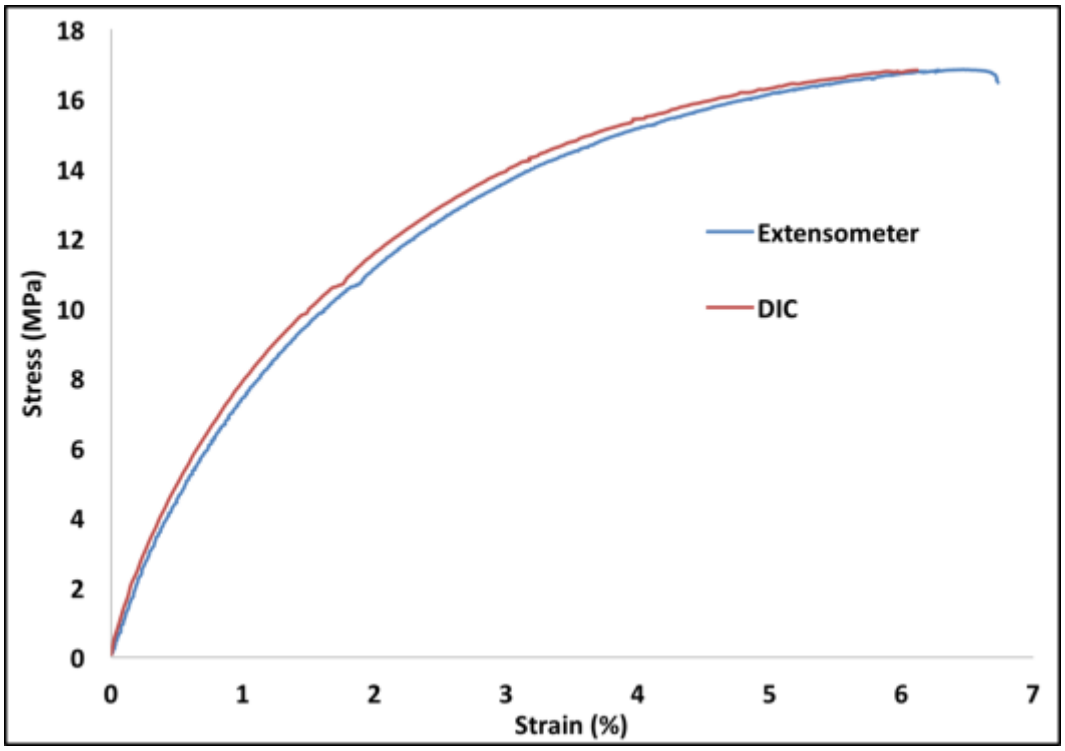

Figure 3-6. Tensile stress-strain data measured by DIC vs extensometer for a representative HDPE pipe section

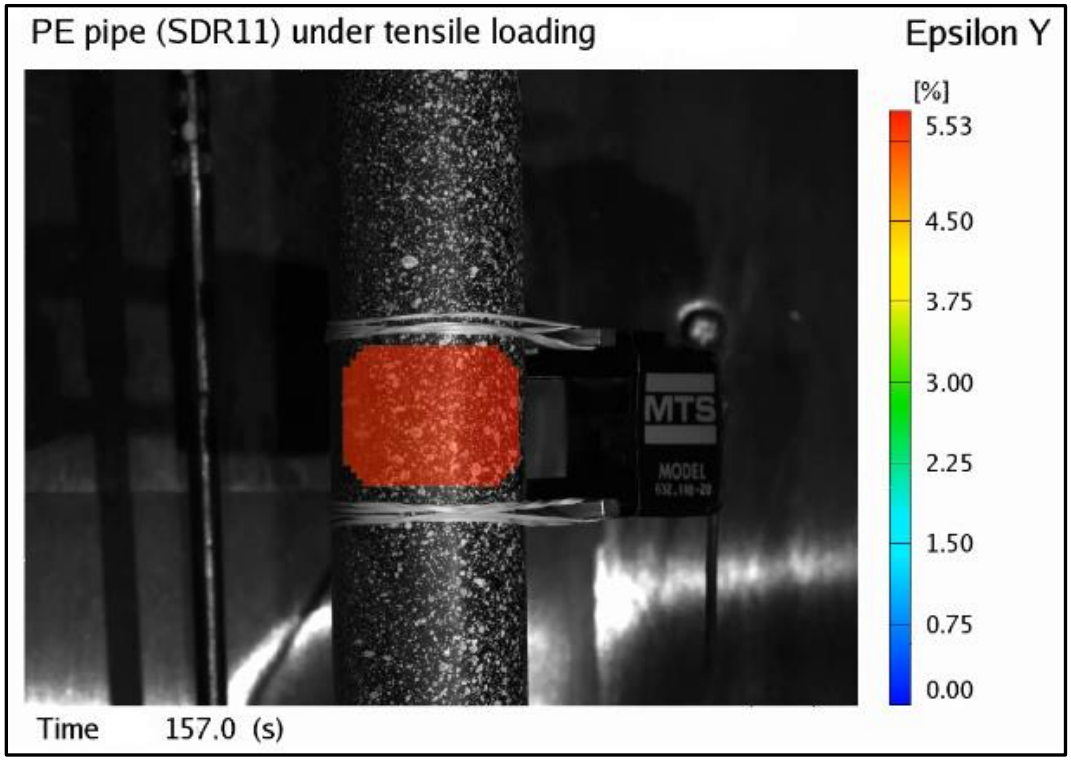

Figure 3-7. Representative HDPE pipe section (SDR 11) under tensile loading

Additionally, a comparison was made to show the difference between the tensile testing and traditional tensile testing which was done on the compression molded dog-bone samples produced by Cincinnati Technology Center of LyondellBasell Industrial Co. Figures 3-9 and 3-10 show the tensile stress-strain results for SDR 11 ODLB1 and ODLB2 pipes which were tested under 10 mm/min tensile loading at 23 °C. The results were compared with the same results for raw materials in the form of compression molded dog-bone samples (bars) for different repetitions. The figures demonstrate the effect of processing and manufacturing conditions on the stress-strain data which shows the possibility of effect of residual stresses present in the pipes. Therefore, using the new designed fixture is able to capture the effects on the raw materials.

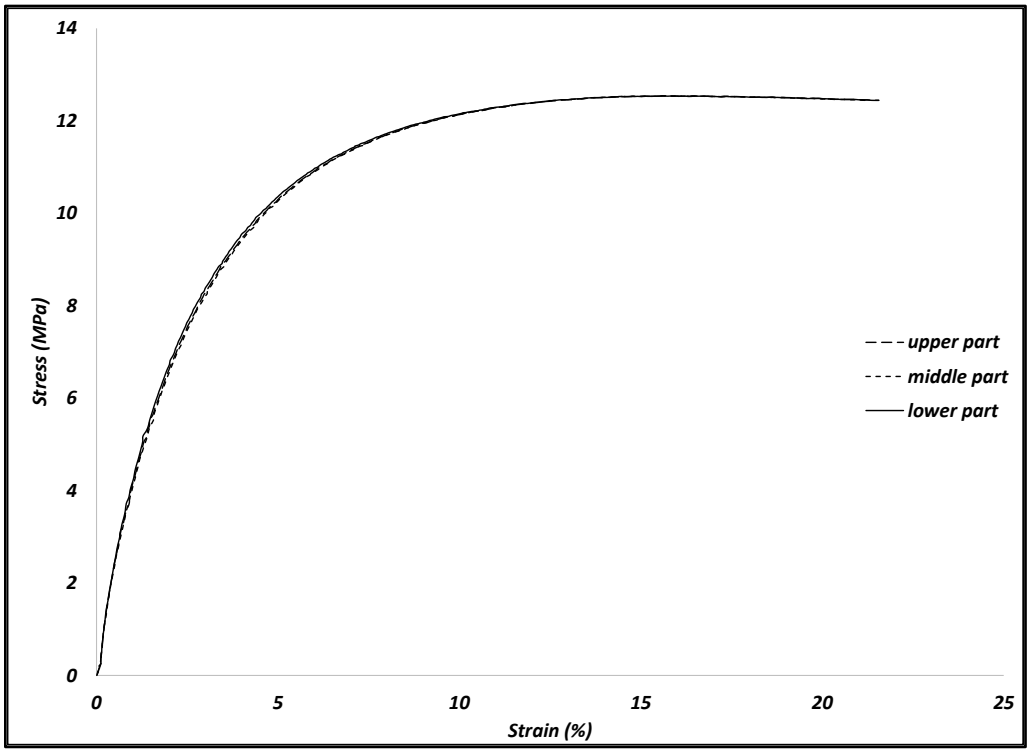

Figure 3-8. NDLB1 pipe section (SDR 11) tensile tested with the rate 10 mm/min under 40 ℃

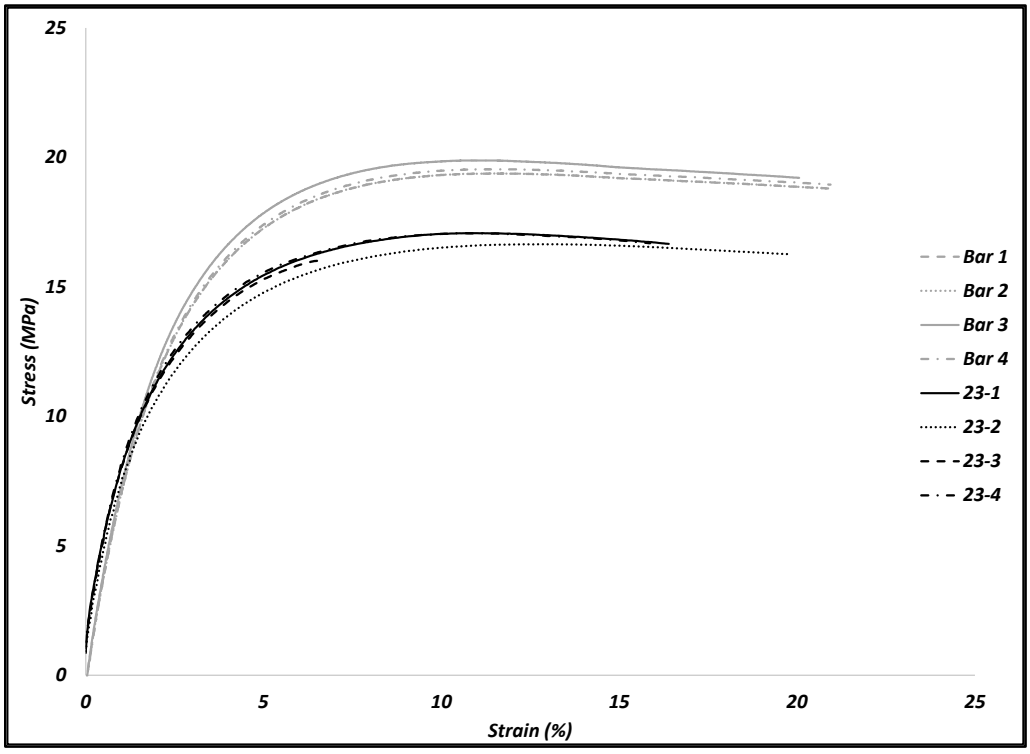

Figure 3-9. ODLB1 pipe section (SDR 11) tensile tested with the rate 10 mm/min under 23 ℃ compared with compression molded dog-bone samples (bars)

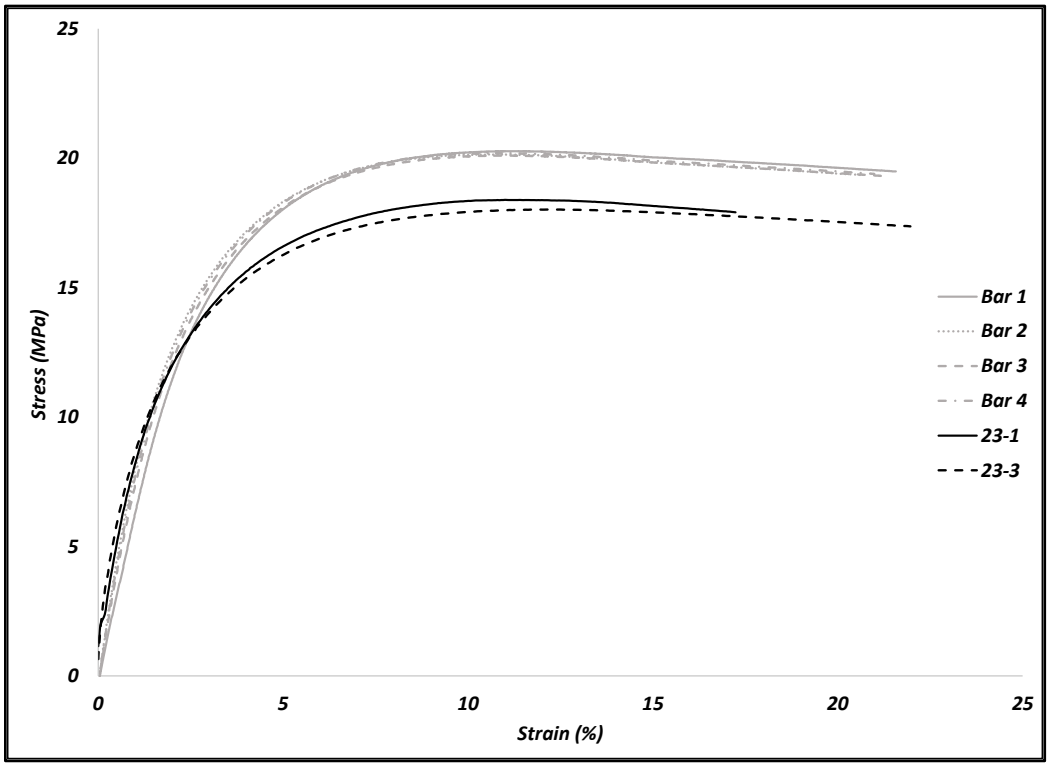

Figure 3-10. ODLB2 pipe section (SDR 11) tensile tested with the rate 10 mm/min under 23 ℃ compared with compression molded dog-bone samples (bars)

Experimental results of compression testing indicate that each of the aspect ratios do not exhibit global buckling under compression loading. Figure 3-11 shows the mode shapes for the wall wrinkling of the samples. However, all except the aspect ratio of 1.2 show barreling effect. Using DIC, the axial strain in different points in the gage length were measured for different aspect ratios. For the aspect ratio 1, the axial strain in different points were in acceptable range during the compression testing.

(a) (b) (c) (d)

Figure 3-11. Four samples of the actual pipe with different aspect ratios (a) 0.6 (b) 0.8 (c) 1, and (d) 1.2

After completing the mechanical testing, tensile yield stress of each configuration (3 different strain rates and 4 different temperatures) and compressive yield stress in 4 different strain rates at the ambient temperature were collected. In addition, the von-Mises strain versus time-to-failure is measured for different configurations (Figure 3-12 represents an example of the burst test results for NDLB2) at different internal pressure levels. Figure 3-12 shows how strain changes with time in the burst test. It includes: (1) primary creep: an initial viscoelastic region, (2) secondary region: which is also called flow regime having a constant strain rate, and (3) tertiary region: in which the strain rate suddenly increases leading to creep rupture. The last region is similar to necking region in tensile testing.

Using the radius and thickness of each pipe and secondary region of the burst test (as an idealized region covering the test), an equivalent stress (von-Mises stress subtracted by the effect of hydrostatic pressure) was calculated vs strain rate (the slope). Furthermore, the time-to-failure and the critical strain in the secondary region were also collected. This eliminates the fourth step proposed by Kanters [4] of performing the creep testing using deadweights to relate the strain rate to the time-to-failure using the calculated critical strain. This could only be achieved using DIC.

Figures 3-13 and 3-14 show the equivalent stress versus strain rate results for different temperatures for LB1 produced by new and old dies compared to the burst test results. The pressure modified Ree-Eyring model is fitted to the data (from tensile and compressive

testing) using minimization of the error function. Table 3-1 and 3-2 show the fitted parameters for the model. The figures show a change in the slope which confirm the observation of Kanters [4] which was mentioned to be related to the two parallel molecular processes for a semi-crystalline polymer. The results for old die shows a good match but the results for the new die presents more conservative results. This could be related to the effect complex residual stress profile in the pipe wall.

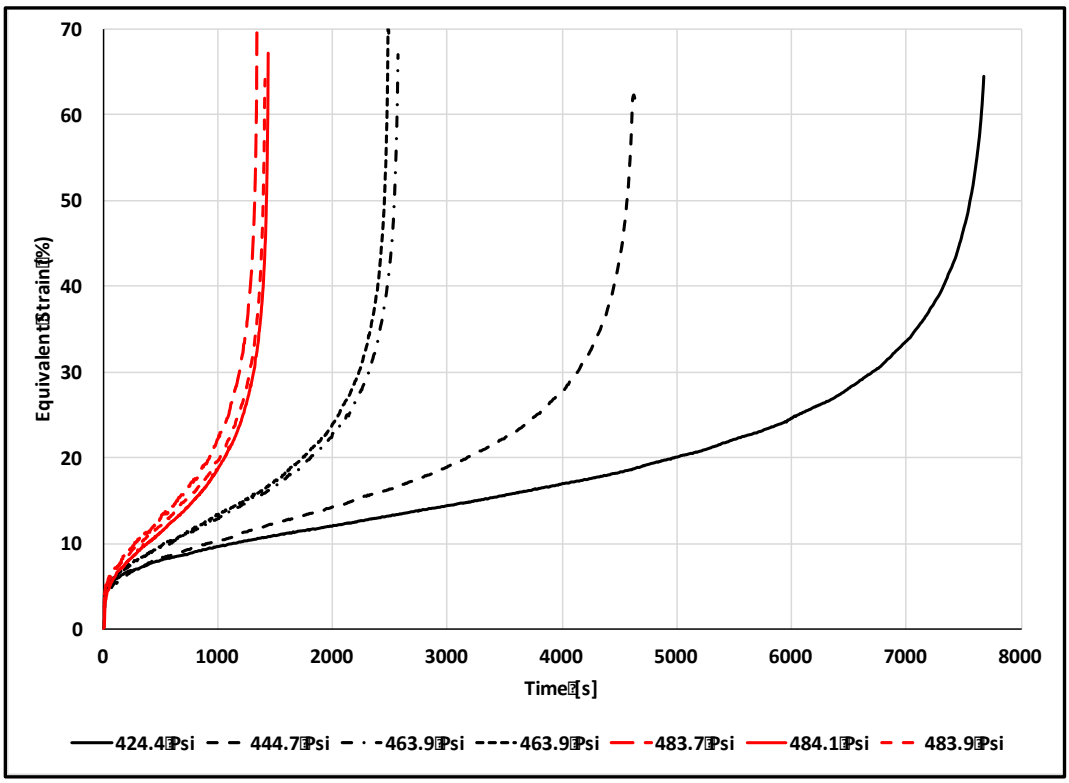

Figure 3-12. Equivalent strain for NDLB1 pipe produced hydrostatic pressure testing

The same data are also represented in figures 3-15 and 3-16 and tables 3-3 and 3-3 for LB2 produced by new and old dies. Both figures show a good match between the model prediction and the burst results.

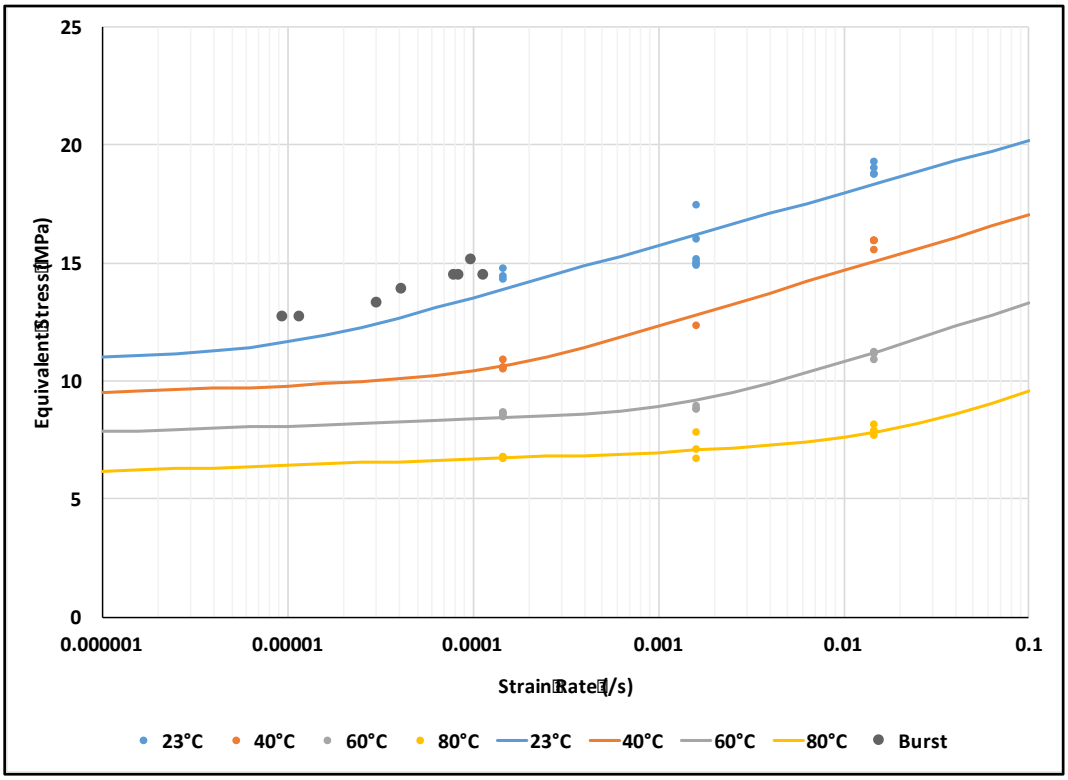

Figure 3-13. Equivalent von-Mises stress subtracted by the hydrostatic pressure term in 4 different temperatures and 3 different strain rates for NDLB1 pipe in addition to the hydrostatic pressure testing data in room temperature. The circle markers show the data from tensile testing and solid lines are the fitted pressure modified Ree-Eyring model

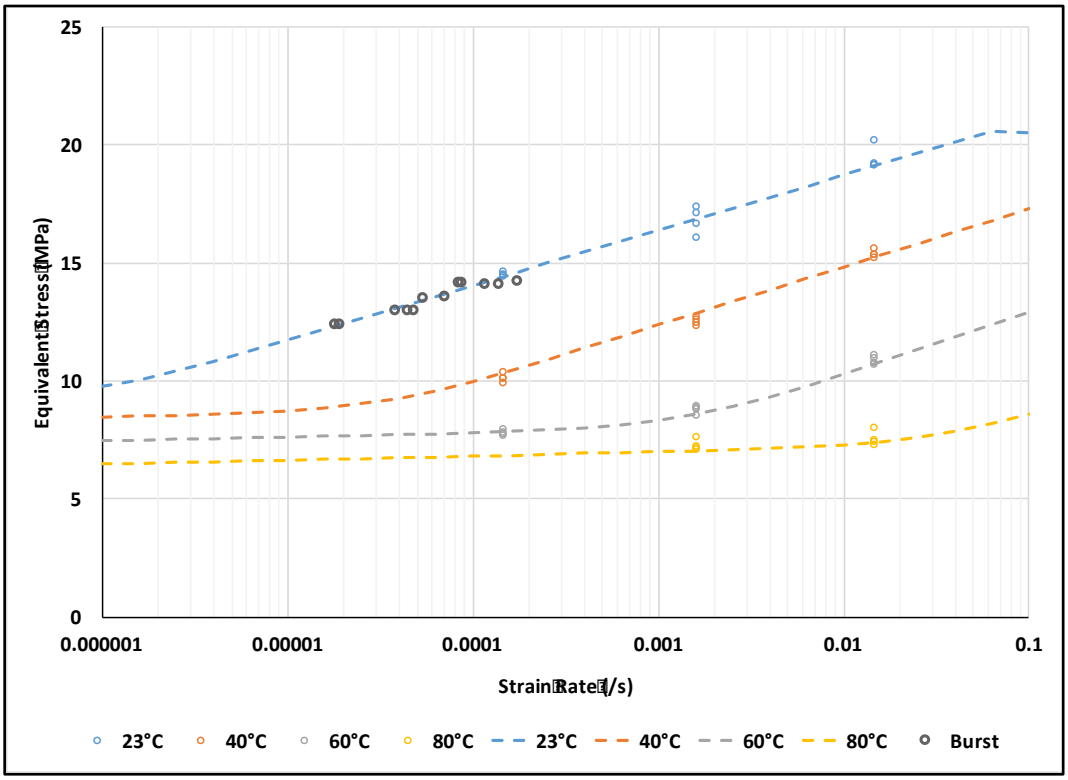

Figure 3-14. Equivalent von-Mises stress subtracted by the hydrostatic pressure term in 4 different temperatures and 3 different strain rates for ODLB1 pipe in addition to the hydrostatic pressure testing data in room temperature. The hollow circle markers show the data from tensile testing and dashed lines are the fitted pressure modified Ree-Eyring model

Table 3-1. Fitted parameters in the pressure modified Ree-Eyring model for NDLB1

Material	i	$V_i^*(\mathrm{nm}^3)$	$\Delta U_i\ (\frac{KJ}{mole})$	$\dot{\varepsilon}_i\ (\frac{1}{s})$	μ
NDLB1	I	37.82	944.85	9.23E+109	0.4802
	II	4.03	111.66	8.8E+14	

Table 3-2. Fitted parameters in the pressure modified Ree-Eyring model for ODLB1

Material	i	$V_i^*(\mathrm{nm}^3)$	$\Delta U_i\ (\frac{KJ}{mole})$	$\dot{\varepsilon}_i\ (\frac{1}{s})$	μ
ODLB1	I	59.68	984	9.4E+99	0.4678
	II	3.7	161.35	5.36E+22	

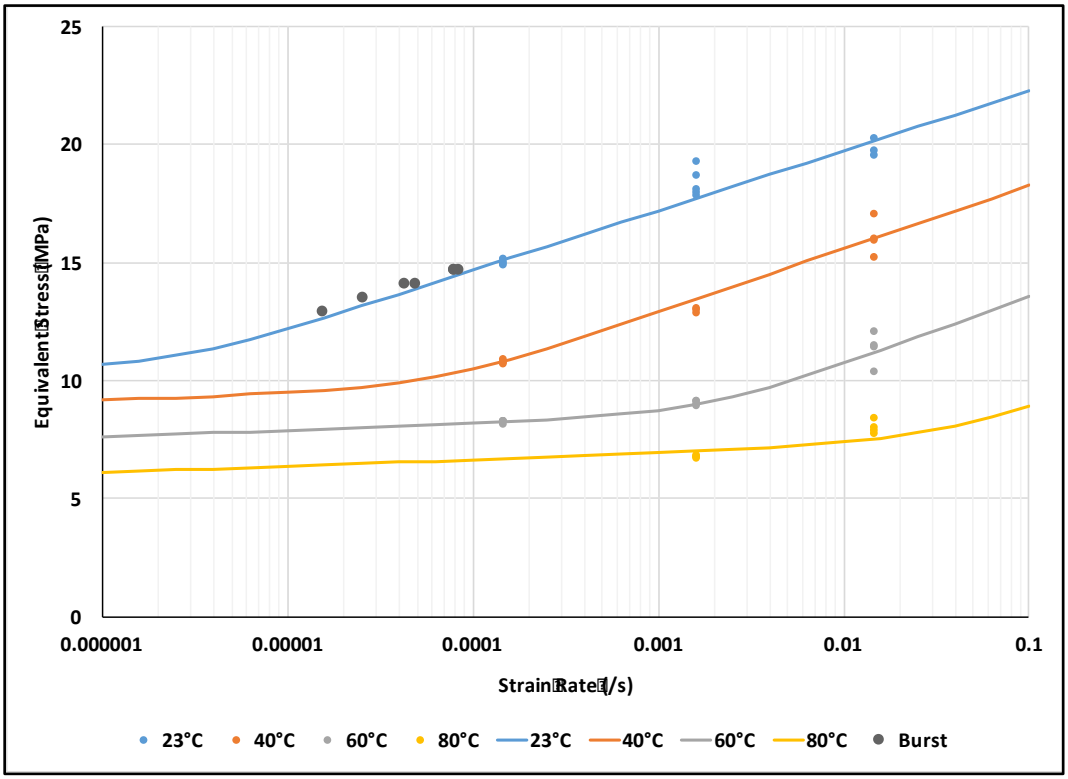

Figure 3-15. Equivalent von-Mises stress subtracted by the hydrostatic pressure term in 4 different temperatures and 3 different strain rates for NDLB2 pipe in addition to the hydrostatic pressure testing data in room temperature. The circle markers show the data from tensile testing and solid lines are the fitted pressure modified Ree-Eyring model

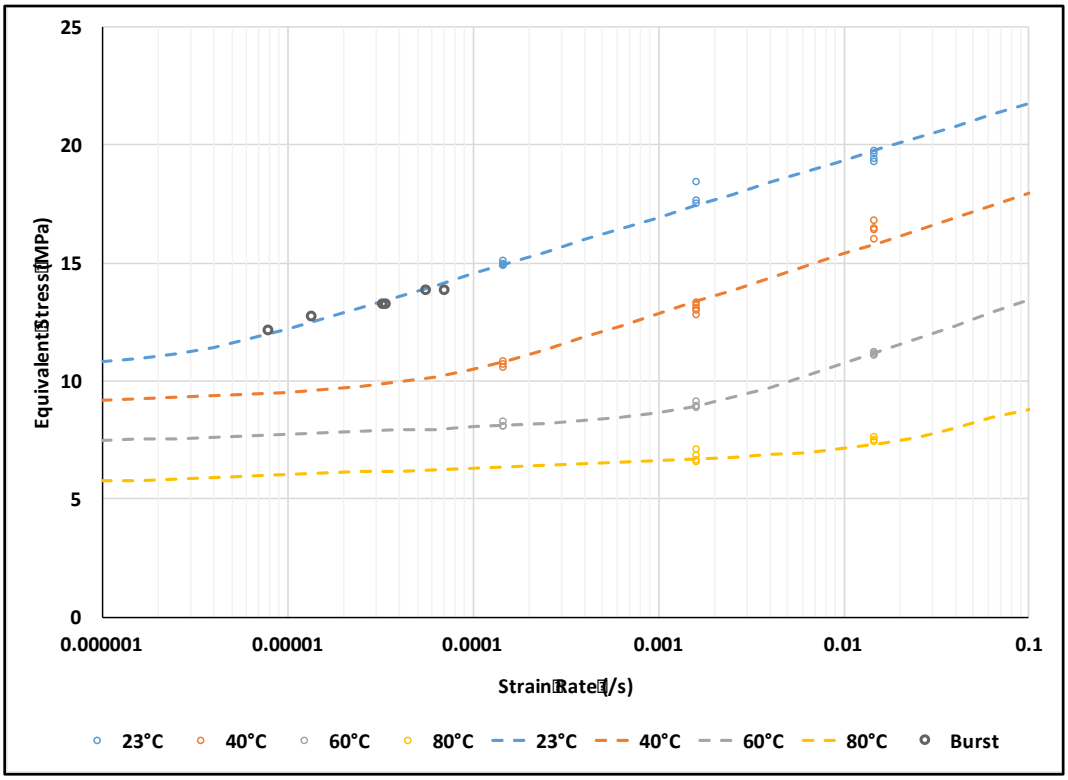

Figure 3-16. Equivalent von-Mises stress subtracted by the hydrostatic pressure term in 4 different temperatures and 3 different strain rates for ODLB2 pipe in addition to the hydrostatic pressure testing data in room temperature. The hollow circle markers show the data from tensile testing and dashed lines are the fitted pressure modified Ree-Eyring model

Table 3-3. Fitted parameters in the pressure modified Ree-Eyring model for NDLB2

Material	i	$V_i^*(\mathrm{nm}^3)$	$\Delta U_i\ (\frac{KJ}{mole})$	$\dot{\varepsilon}_i\ (\frac{1}{s})$	μ
NDLB2	I	36.13	8605.76	4.13E+91	0.352
	II	3.66	145	1.82E+20	

Table 3-4. Fitted parameters in the pressure modified Ree-Eyring model for ODLB2

Material	i	$V_i^*(\mathrm{nm}^3)$	$\Delta U_i\ (\frac{KJ}{mole})$	$\dot{\varepsilon}_i\ (\frac{1}{s})$	μ
ODLB2	I	35.12	869.12	2.71E+102	0.4153
	II	3.8	136.46	6.45E+18	

Chapter 4

4. Conclusion and future work

4.1. Conclusion

In this study, a new accelerated creep characterization approach is introduced for HDPE (as a microscopically heterogeneous semi-crystalline polymers) pipes which considers the effect of processing conditions and structure using the Ree-Eyring modification of pressure-modified Eyring flow condition in addition to assumption of existing a critical amount of accumulated plastic strain for failure. The approach captures plastic flow kinetics and is to predict the long-term behavior of HDPE pipes based on their short-term behavior (yield stress which is strain and temperature dependent). To complete the approach, custom designed fixtures were developed to do tensile and hoop testing on the pipe sections to account for the effect of processing conditions. Subsequently, mechanical properties of HDPE pipe sections were measured under tensile and hydrostatic pressure loading with Digital Image Correlation (DIC) used to measure deformations at different temperatures and strain rates. The dependence of yield stress to temperature and strain rate for the pipes was decomposed into two parallel molecular processes which were due to (1) intralamellar deformation because of crystal slip at higher temperatures and low strain rates and (2) α-transition (interlamellar deformation). As a result, rupture lifetime of HDPE pipes were predicted using a combination of experimental results and pressure modified Ree-Eyring flow equation which potentially is able to decrease the creep characterization time from 13 months to approximately one week.

4.2. Future work

It was explained that the homogenous and heterogonous slip processes may introduce two yielding points in the true stress-strain data depending on the temperature, strain rate of the experiment, and hydrostatic pressure. The second yield point is the reason for the visible necking in the tensile testing but the first yield may lead to a local yielding which is

not obvious because of the subsequent strong strain hardening process. It was previously observed [27] that, depending on the temperature and strain rate of experiment, the first or the second yielding processes may be the maximum point in the engineering stress-strain data. However, in the modeling process, the maximum point in engineering stress-strain data was chosen as the yielding point for both tensile and compression testing. The effect and the role of each yielding can be studied to see which yielding in responsible for the creep rupture. This can be accomplished by studying the polymer structure at rupture failure and comparing that with the polymer structure at tensile and compression yielding using SAXS and WAXD [33, 34].

It was observed in experiments that recognizing the two yield points in true stress-strain figures is difficult and even sometimes impossible. Therefore, a systematic technique should be developed that could be used for all tensile and compressive data.

In yield stress versus log strain rate data, the change in slope was claimed to be related to α-relaxation process. A clear relationship between α-relaxation and the point of change in slope which is strain rate and temperature dependent may help to further simplify the modeling process. The α-relaxation temperature is usually measured with Dynamic Mechanical Analysis (DMA). Sample receives 3°C/min heating at 1 Hz, with 0.1% strain (to be in linear viscoelastic region), from -150 °C all the way to the highest temperature, T_m. Transitions are labeled on the $\tan(\delta)$ from right to left, starting with alpha and moving toward the left (beta, then gamma, if materials exhibit that). Therefore, α-relaxation temperature is obviously, strain rate and applied stress dependent.

To prove the idea of predicting the strain rate based on short term testing, each configuration was tested at least four times for a specific temperature and strain rate to make sure the yield results are repeatable. Based on the results, it was confirmed that the results have very low standard deviation but that led into having less data points in the yield stress versus strain rate figures and for the fitting process. Therefore, doing just one test but for more combination of temperature and strain rate may result in better fit of Ree-Eyring parameters.

5. References

1. *Global Ductile Iron Pipe Sales 2015 Market Research Report.* p. 165.
2. Zhang, J., *Experimental study of stress cracking in high density polyethylene pipes*. 2005, Drexel University.
3. *Basell-Materials for Pipe extrusion.* 2014.
4. Kanters, M., *Prediction of Long-Term Performance of Load-Bearing Thermoplastics*. 2015, Technische Universiteit Eindhoven.
5. Colin, X., et al., *Aging of polyethylene pipes transporting drinking water disinfected by chlorine dioxide. Part II—Lifetime prediction.* Polymer Engineering & Science, 2009. **49**(8): p. 1642-1652.
6. Sanders, J., et al., *Methods for determining the in-service life of polymer water pipes.* Journal of materials science, 2009. **44**(17): p. 4683-4691.
7. Cheng, J.J., *Mechanical and chemical properties of high density polyethylene: Effects of microstructure on creep characteristics*. 2008, University of Waterloo.
8. Staff, *Mechanical Behavior of Materials Laboratory Manual*. 2012, Blacksburg, VA: Virginia Tech.
9. *ASTM D2837-13e1: Standard Test Method for Obtaining Hydrostatic Design Basis for Thermoplastic Pipe Materials or Pressure Design Basis for Thermoplastic Pipe Products.*
10. ISO, E., *9080.* Plastics piping and ducting systems–determination of the long-term hydrostatic strength of thermoplastics materials in pipe form by extrapolation, 2003.
11. Mathot, V. and M. Pijpers, *Heat capacity, enthalpy and crystallinity of polymers from DSC measurements and determination of the DSC peak base line.* Thermochimica acta, 1989. **151**: p. 241-259.
12. Hagemann, H., et al., *Quantitative infrared methods for the measurement of crystallinity and its temperature dependence: polyethylene.* Macromolecules, 1989. **22**(9): p. 3600-3606.
13. Kitamaru, R., F. Horii, and K. Murayama, *Phase structure of lamellar crystalline polyethylene by solid-state high-resolution carbon-13 NMR detection of the crystalline-amorphous interphase.* Macromolecules, 1986. **19**(3): p. 636-643.
14. Litvinov, V. and M. Soliman, *The effect of storage of poly (propylene) pipes under hydrostatic pressure and elevated temperatures on the morphology, molecular mobility and failure behaviour.* Polymer, 2005. **46**(9): p. 3077-3089.
15. Sun, N., M. Wenzel, and A. Adams, *Morphology of high-density polyethylene pipes stored under hydrostatic pressure at elevated temperature.* Polymer, 2014. **55**(16): p. 3792-3800.
16. Cazenave, J., et al., *Short-term mechanical and structural approaches for the evaluation of polyethylene stress crack resistance.* Polymer, 2006. **47**(11): p. 3904-3914.
17. Cherry, B. and T.S. Hin, *Energy criterion for modelling creep rupture of high-density polyethylene.* Polymer, 1983. **24**(8): p. 1067-1070.
18. Barton, S.J. and B.W. Cherry, *Predicting the Creep-Rupture Life of Polyethylene Pipe.* Polymer Engineering and Science, 1979. **19**(8): p. 590-595.
19. Eyring, H., S. Glasstone, and K.J. Laidler, *The theory of rate processes.* McGrow-Hill Book, New York, 1941.
20. Coleman, B.D., *Application of the theory of absolute reaction rates to the creep failure of polymeric filaments.* Journal of Polymer Science, 1956. **20**(96): p. 447-455.

21. Sherby, O.D., *Factors affecting the high temperature strength of polcyrystalline solids.* Acta Metallurgica, 1962. **10**(2): p. 135-147.
22. Furillo, F., S. Purushothaman, and J. Tien, *Understanding the Larson-Miller Parameter.* Scripta Metallurgica, 1977. **11**(6): p. 493-496.
23. Rosen, B., *Fracture processes in polymeric solids: phenomena and theory*. 1964: Interscience Publishers.
24. Fotheringham, D. and B. Cherry, *The role of recovery forces in the deformation of linear polyethylene.* Journal of Materials Science, 1978. **13**(5): p. 951-964.
25. Lai, J. and A. Bakker, *Analysis of the non-linear creep of high-density polyethylene.* Polymer, 1995. **36**(1): p. 93-99.
26. Gates, T.S., D.R. Veazie, and L.C. Brinson, *Creep and Physical Aging in a Polymeric Composite: Comparison of Tension and Compression.* Journal of Composite Materials, 1997. **31**(24): p. 2478-2505.
27. Sedighiamiri, A., L. Govaert, and J. Van Dommelen, *Micromechanical modeling of the deformation kinetics of semicrystalline polymers.* Journal of Polymer Science Part B: Polymer Physics, 2011. **49**(18): p. 1297-1310.
28. Boyd, R.H., *Relaxation processes in crystalline polymers: experimental behaviour—a review.* Polymer, 1985. **26**(3): p. 323-347.
29. Boyd, R.H., *Relaxation processes in crystalline polymers: molecular interpretation—a review.* Polymer, 1985. **26**(8): p. 1123-1133.
30. Seguela, R., S. Elkoun, and V. Gaucher-Miri, *Plastic deformation of polyethylene and ethylene copolymers: Part II Heterogeneous crystal slip and strain-induced phase change.* Journal of materials science, 1998. **33**(7): p. 1801-1807.
31. Séguéla, R., V. Gaucher-Miri, and S. Elkoun, *Plastic deformation of polyethylene and ethylene copolymers: Part I Homogeneous crystal slip and molecular mobility.* Journal of materials science, 1998. **33**(5): p. 1273-1279.
32. Crist, B., C.J. Fisher, and P.R. Howard, *Mechanical properties of model polyethylenes: tensile elastic modulus and yield stress.* Macromolecules, 1989. **22**(4): p. 1709-1718.
33. Butler, M.F., A.M. Donald, and A.J. Ryan, *Time resolved simultaneous small-and wide-angle X-ray scattering during polyethylene deformation—II. Cold drawing of linear polyethylene.* Polymer, 1998. **39**(1): p. 39-52.
34. Butler, M.F., A.M. Donald, and A.J. Ryan, *Time resolved simultaneous small-and wide-angle X-ray scattering during polyethylene deformation 3. Compression of polyethylene.* Polymer, 1998. **39**(4): p. 781-792.
35. Sedighiamiri, A., et al., *Micromechanics of semicrystalline polymers: Yield kinetics and long-term failure.* Journal of Polymer Science Part B: Polymer Physics, 2012. **50**(24): p. 1664-1679.
36. Bowden, P. and R. Young, *Deformation mechanisms in crystalline polymers.* Journal of Materials Science, 1974. **9**(12): p. 2034-2051.
37. Lee, B., et al., *Simulation of large strain plastic deformation and texture evolution in high density polyethylene.* Polymer, 1993. **34**(17): p. 3555-3575.
38. Lee, B., D. Parks, and S. Ahzi, *Micromechanical modeling of large plastic deformation and texture evolution in semi-crystalline polymers.* Journal of the Mechanics and Physics of Solids, 1993. **41**(10): p. 1651-1687.

39. Van Dommelen, J., et al., *Micromechanical modeling of the tensile behavior of oriented polyethylene.* Journal of Polymer Science Part B: Polymer Physics, 2004. **42**(16): p. 2983-2994.
40. Truss, R., et al., *The dependence of yield behavior on temperature, pressure, and strain rate for linear polyethylenes of different molecular weight and morphology.* Journal of Polymer Science: Polymer Physics Edition, 1984. **22**(2): p. 191-209.
41. Bauwens, J., *Yield condition and propagation of Lüders' lines in tension–torsion experiments on poly (vinyl chloride).* Journal of Polymer Science Part A-2: Polymer Physics, 1970. **8**(6): p. 893-901.
42. Bauwens-Crowet, C., J.-C. Bauwens, and G. Homes, *The temperature dependence of yield of polycarbonate in uniaxial compression and tensile tests.* Journal of Materials Science, 1972. **7**(2): p. 176-183.
43. Bauwens-Crowet, C., *The compression yield behaviour of polymethyl methacrylate over a wide range of temperatures and strain-rates.* Journal of Materials Science, 1973. **8**(7): p. 968-979.
44. Bauwens-Crowet, C., J.-M. Ots, and J.-C. Bauwens, *The strain-rate and temperature dependence of yield of polycarbonate in tension, tensile creep and impact tests.* Journal of Materials Science, 1974. **9**(7): p. 1197-1201.
45. Crissman, J. and G. McKenna, *Relating creep and creep rupture in PMMA using a reduced variable approach.* Journal of Polymer Science Part B: Polymer Physics, 1987. **25**(8): p. 1667-1677.
46. Eyring, H., *Viscosity, plasticity, and diffusion as examples of absolute reaction rates.* The Journal of chemical physics, 1936. **4**(4): p. 283-291.
47. Ward, I.M., *Review: The yield behaviour of polymers.* Journal of materials Science, 1971. **6**(11): p. 1397-1417.
48. Ree, T. and H. Eyring, *Theory of Non-Newtonian Flow. II. Solution System of High Polymers.* Journal of Applied Physics, 1955. **26**(7): p. 800-809.
49. Mears, D., K. Pae, and J. Sauer, *Effects of hydrostatic pressure on the mechanical behavior of polyethylene and polypropylene.* Journal of Applied Physics, 1969. **40**(11): p. 4229-4237.
50. Spitzig, W. and O. Richmond, *Effect of hydrostatic pressure on the deformation behavior of polyethylene and polycarbonate in tension and in compression.* Polymer Engineering & Science, 1979. **19**(16): p. 1129-1139.
51. Aidi, B. and S.W. Case, *Experimental and Numerical Analysis of Notched Composites Under Tension Loading.* Applied Composite Materials, 2015. **22**(6): p. 837-855.